

Discovery and Timing of 49 Pulsars from the Arecibo 327-MHz Drift Survey

TIMOTHY E. E. OLSZANSKI,^{1,2} EVAN F. LEWIS,^{1,2} JULIA S. DENEVA,³ MAURA A. MCLAUGHLIN,^{1,2} KEVIN STOVALL,⁴
PAULO C. C. FREIRE,⁴ BENETGE B. P. PERERA,⁵ MANJARI BAGCHI,^{6,7} AND JOSE G. MARTINEZ⁴

¹*Department of Physics and Astronomy, West Virginia University, P.O. Box 6315, Morgantown, WV 26506, USA*

²*Center for Gravitational Waves and Cosmology, West Virginia University, Chestnut Ridge Research Building, Morgantown, WV 26506, USA*

³*George Mason University, Fairfax, VA 22030, USA*

⁴*Max-Planck-Institut für Radioastronomie, Bonn, Germany*

⁵*Florida Space Institute, University of Central Florida, 12354 Research Parkway, Orlando, FL 32826, USA*

⁶*The Institute of Mathematical Sciences, Chennai, India 600113*

⁷*Homi Bhabha National Institute, Mumbai, India 400094*

(Received June 1, 2019; Revised January 10, 2019; Accepted February 10, 2025)

ABSTRACT

We present 18 pulsar discoveries from the AO327 pulsar survey, along with their timing solutions and those for an additional 31 AO327-discovered pulsars. Timing solutions were constructed using observations from a follow-up timing campaign taken between the periods of 2013 — 2019 using the Arecibo Observatory’s 327-MHz receiver. Aside from PSR J0916+0658, an isolated pulsar that shows evidence for partial recycling, the remaining discoveries are non-recycled pulsars. We present a brief census of emission features for all pulsars with the following standouts. PSR J1942+0142 is found to exhibit the very rare phenomenon of subpulse bi-drifting and PSR J0225+1727 has an interpulse. We also report distance estimates using the NE2001 and YMW16 Galactic electron density models, and identify at least 10 sources where either one or both models underestimate the maximum Galactic line of sight dispersion measure.

Keywords: editorials, notices — miscellaneous — catalogs — surveys

1. INTRODUCTION

Since their discovery by Jocelyn Bell over 50 years ago (Hewish et al. 1968), radio pulsars have proven themselves to be immensely useful astrophysical laboratories. They have provided a number of fundamental physics advancements, the most prominent of which are evidence for a nanohertz gravitational wave background via the use of pulsar timing arrays (PTAs, Agazie et al. 2023), tests of general relativity (GR) and fundamental properties of gravity (e.g., Kramer et al. 2021, for a general review see Freire & Wex 2024), and tests of the properties of the strong nuclear force via their equation of state (EOS, Özel & Freire 2016; Lattimer 2021). A number of open questions involving pulsars remain, such as the nature of their radio emission and corre-

sponding fundamental plasma physics (Harding 2017), pulsar and neutron star populations and their consequences for stellar evolution (Lorimer et al. 2019), stellar evolution in binaries (Tauris et al. 2017; Tauris & van den Heuvel 2023), and the properties of the interstellar medium (Turner et al. 2021).

Although more than 3,600 radio pulsars are known¹ (Manchester et al. 2005), extensive pulsar surveys carried out world-wide (e.g., Manchester et al. 2001; Cordes et al. 2006; Keith et al. 2010; Stovall et al. 2014; Han et al. 2021; Ridolfi et al. 2021) continue to produce new discoveries. In the last decade alone, these include ultra long period pulsars (Caleb et al. 2022; Sob’yanin 2023), high-mass pulsars (Cromartie et al. 2020; Fonseca et al. 2021), highly relativistic binary systems (Pan et al. 2023) and possibly the first pulsar - black hole system (Barr et al. 2024). The Five-hundred-meter Aperi-

Corresponding author: Timothy E. E. Olszanski
teo0008@mix.wvu.edu

¹ <https://www.atnf.csiro.au/research/pulsar/psrcat/>

Discovery name (J2000)	Final name (J2000)	P (s)	DM (pc cm^{-3})	Binary?	Discovery date (yyyy mm dd)	Pipeline(s)	Reference
J0011+08	J0011+0805	2.55287	24.8		2014 05 21	FFT, SP	(6), (12)
J0050+03	J0050+0348	1.36656	26.4		2014 05 22	FFT, SP	(6), (12)
	J0154+1833	0.00236	19.8		2013 09 11	FFT	(9)
J0156+04			27.5	?	2014 05 20	SP	(6)
J0158+21	J0158+2106	0.50528	19.9		2012 08 30	FFT	(2), (12)
	J0225+1727	0.39031	20.0		2013 09 15	FFT, SP	(12)
J0229+20	J0229+2058	0.80688	26.7		2012 09 03	FFT, SP	(2), (12)
J0241+16	J0241+1604	1.54530	19.6		2005 04 03	FFT, SP	(2), (12)
J0244+14	J0245+1433	2.12748	29.5		2012 08 10	FFT, SP	(2), (12)
	J0354+0847	0.99888	66.0		2015 04 30	FFT, SP	
J0453+16	J0453+1559	0.04578	30.3	yes	2012 08 10	FFT	(2), (4)
J0457+23	J0457+2333	0.50491	58.7		2012 08 19	FFT, SP	(2), (12)
J0509+08	J0509+0856	0.00406	38.3	yes	2013 04 18	FFT	(2), (9)
J0544+20			56.9	?	2014 02 07	SP	(6)
J0550+09		1.745	86.6	?	2014 10 15	SP	(6)
J0608+00	J0608+0044	1.07619	48.4		2012 10 06	FFT, SP	(2), (12)
J0611+04	J0611+0411	1.67443	69.6		2014 02 03	FFT, SP	(6), (12)
J0628+06	J0627+0649	0.34652	86.5		2012 11 26	FFT	(1)*, (12)
J0630+19		1.24855	48.3		2015 04 09	FFT, SP	(6)
	J0639-0004	2.40949	70.1		2013 01 22	FFT, SP	(12)
	J0709+0458	0.03443	44.3	yes	2013 10 21	FFT	(9)
	J0732+2314	0.00409	44.7	yes	2016 10 07	FFT	(9)
J0806+08	J0806+0811	2.06310	46.7		2013 06 18	FFT, SP	(2), (12)
J0824+00	J0824+0028	0.00986	34.5	yes	2012 10 27	FFT	(2), (9)
J0848+16	J0848+1640	0.45226	38.6		2006 06 20	FFT, SP	(2), (12)
	J0916+0658	0.04477	19.2		2017 06 22	FFT	(12)
J0928+06	J0928+0614	2.06036	50.5		2013 07 01	FFT, SP	(2), (12)
J1010+15			42.2	?	2012 10 27	SP	(2)
	J1147+0829	1.62478	26.9		2014 04 28	FFT, SP	(12)
	J1215+3058	0.83596	15.6		2016 11 10	FFT, SP	(12)
	J1411+2551	0.06245	12.4	yes	2014 09 09	FFT	(7)
J1433+00			23.6	?	2014 07 18	SP	(6)
	J1531+0519	1.41982	31.3		2017 04 27	FFT, SP	(12)
	J1538+1736	0.69024	34.6		2014 09 01	FFT	(12)
J1554+18			24.0		2014 09 13	SP	(6)
J1603+18		0.503	29.7	?	2014 09 16	SP	(6)
	J1628+0613	1.67847	53.9		2013 10 20	FFT, SP	(12)
	J1630+3550	0.00323	17.5	yes	2018 01 17	FFT	(11)
	J1637+1131	1.67847	53.9		2013 11 27	FFT, SP	(12)
J1656+00	J1656+0018	1.49785	47.4		2014 08 05	FFT, SP	(6), (12)
J1717+03		3.901	25.6	?	2014 01 22	SP	(6)
J1720+00		3.357	46.2	?	2014 05 20	SP	(6)
J1726-00	J1726-0022	1.30862	59.9		2013 03 24	FFT	(2), (12)
J1738+04	J1738+0418	1.39179	23.5		2014 10 15	FFT, SP	(6), (12)
	J1742+2022	0.25258	19.8		2016 04 05	FFT, SP	
J1743+05	J1743+0532	1.47364	55.4		2014 05 21	FFT, SP	(6), (12)
J1749+16	J1749+1629	2.31132	59.5		2014 10 23	FFT, SP	(6), (12)
J1750+07	J1750+0733	1.90881	55.7		2014 05 08	FFT, SP	(6), (12)
J1802+03	J1802+0344	0.66426	76.9		2013 01 13	FFT	(2), (12)
J1807+04	J1807+0359	0.79885	52.7		2012 10 20	FFT, SP	(2), (12)
J1821+01					2012 10 31	FFT	(2), (3)*
	J1832+2749	0.63170	47.4		2014 10 14	FFT	(12)
	J1845+3543						
	J1912+1947	2.37616	94.2		2014 07 16	FFT, SP	(12)
	J1917+3115	1.84024	81.1		2016 11 11	FFT, SP	(12)
J1937-00	J1937-0023	0.24015	67.9		2013 07 11	FFT	(2), (12)
J1938+14	J1938+1505	2.90251	74.4		2014 10 23	FFT, SP	(6), (12)
J1941+01	J1942+0147	1.40473	133.2		2014 05 15	FFT, SP	(6), (12)
J1945+07	J1945+0720	1.07394	62.3		2012 10 11	FFT, SP	(2), (12)
J1946+14	J1946+1447	2.28244	50.5		2014 10 23	FFT, SP	(6), (12)
J1956+07	J1957+0724	5.01248	61.8		2015 05 01	FFT, SP	(6), (12)
	J2050+1820	5.0483	63.1		2013 09 10	FFT, SP	(12)
	J2055+1545	0.00216	30.3	yes	2016 02 16	FFT	(11)
	J2059+1100	0.95389	60.3		2014 10 10	FFT	(12)
J2105+07	J2105+0757	3.74663	52.5		2014 09 15	FFT, SP	(6), (12)
	J2116+1345	0.00222	30.3	yes	2016 02 29	FFT	(11)
	J2151+1918	1.03372	30.9		2016 04 19	FFT, SP	(12)
	J2202+2134	1.35727	17.8		2017 05 01	FFT, SP	(8)*, (12)
J2204+27	J2204+2700	0.08470	35.1	yes	2011 08 24	FFT	(2), (9)
	J2212+2450	0.00391	30.3		2017 11 10	FFT	(11)
J2234+06	J2234+0611	0.00358	10.8	yes	2013 01 04	FFT	(2), (5), (10)
	J2252+2455	1.79762	34.8		2017 09 18	FFT, SP	(12)
J2329+16	J2329+1657	0.63207	30.4		2013 04 04	FFT, SP	(2), (12)
J2340+08	J2340+0831	0.30330	23.8		2012 10 14	FFT, SP	(2), (12)
	J2347+0300	1.38347	16.1		2016 03 01	FFT, SP	(12)
	J2354+0434	0.95635	12.6		2016 02 23	FFT, SP	(12)

Table 1. Published pulsar discoveries (including this work) from the AO327 survey. Column 1–2 indicate initial and, where applicable, final pulsar name from the timing solution localizations. Columns 3–5 list basic properties (spin period, DM, binary status). In some cases (specified with question marks) the binary status is not yet known because no precise periodicities and/or phase-connected timing solutions have been derived. Column 6–7 indicates discovery dates and which pipelines yielded detections (FFT and or single-pulse). Lastly, column 8 provides the latest references on these pulsars. Those indicated with asterisks were independently co-discovered by other teams. References by date of publication are: (1) Burgay et al. (2012), (2) Deneva et al. (2013), (3) Rosen et al. (2013), (4) Martinez et al. (2015), (5) Antoniadis et al. (2016), (6) Deneva et al. (2016), (7) Martinez et al. (2017), (8) Tyulbashev, V. S. & Malofeev, V. M. (2018), (9) Martinez et al. (2019), (10) Stovall et al. (2019), (11) Lewis et al. (2023), (12) this work.

ture Spherical Telescope (FAST) in China has discovered around 600 new pulsars in only a few years of operation². Another major impetus for ongoing pulsar surveys is to find suitable sources that can support the efforts of PTAs (Alam et al. 2020; Perera et al. 2019; Chen et al. 2021; Kerr et al. 2020). With the recent evidence for nanohertz gravitational waves presented by the NANOGrav collaboration (Agazie et al. 2023) and other PTAs (Agazie et al. 2024; EPTA Collaboration and InPTA Collaboration et al. 2023; Reardon et al. 2023), pulsar surveys serve an ever more valuable role by identifying sources well-suited for PTA inclusion.

The radio sky is not limited only to pulsars. Surveys are sensitive to transient sources such as fast radio bursts (FRBs, Cordes & Chatterjee 2019), which originate from outside the Galaxy, rotating radio transients (RRATs, McLaughlin et al. 2006; Keane et al. 2011; Thornton et al. 2013) though their single pulses, and ultra long period transients (Caleb et al. 2024). New survey discoveries help to improve the census of neutron stars as well as the modeling of the Galaxy’s free electron distribution. In particular, low-frequency surveys are especially sensitive to both nearby and distant pulsars. This is because most pulsars’ spectra peak below 500 MHz. While the increasing effects of dispersion toward lower frequencies favors detection of fainter nearby sources, we also remain sensitive to bright distant sources along lines of sight with lower electron densities. The latter being very useful for probing the limitations of current electron density models, and which in turn are useful for refining distance estimates for FRBs. With its unmatched sensitivity to the faintest sources, Arecibo was an ideal telescope for this work.

Pulsars are detected most commonly in the radio band due to the coherent nature of radio emission. Broadly, pulsars divide into two classes as shaped by their history of accretion. Pulsars where significant accretion has taken place have shorter spin periods as compared to younger, non-recycled or slow pulsars. In most cases, accretion modifies the structure of milli-second pulsar (MSP) magnetospheres, and by extension emission regions. As a consequence, MSP profiles are typically more complex. Therefore, non-recycled pulsars provide a simpler window into the physics that drives the emission process. Their radio emission is characterized by a rich collection of behaviors that in turn reflect the physical conditions of the underlying fundamental magnetospheric plasma physics. Broadly, these behaviors can be subdivided into two categories; those that involve ampli-

tude modulation of some form e.g. nulling, giant pulses, mode changing, periodic emission etc, (Wang et al. 2007; Johnston & Romani 2004; Ng et al. 2020; Basu et al. 2020), and those that relate to apparent motion of emission across the beam such as subpulse drift (Basu et al. 2018). While some MSPs show some of these behaviors (Mahajan et al. 2018; Palliyaguru et al. 2023), most MSPs do not have detectable single pulses, making them much more difficult to study. Studies of these behaviors serve as useful observational constraints for theorists.

The Arecibo Observatory (AO) 327-MHz Drift Survey (AO327, Deneva et al. 2013) began in 2010 and ended in December 2020, making use of time when the 305-m telescope was not fully functional, such as during repairs or under tropical storm watch, as well as under-subscribed local sidereal time ranges (LSTs). A “drift” scan is performed by positioning the telescope at a fixed azimuth and zenith angle, and allowing the sky to pass overhead. Due to the tragic collapse of Arecibo in December 2020, the AO327 survey ended before completing its intended sky coverage, with 65% of the Arecibo sky observed, as shown in Fig. 1. The complete dataset has been processed through our search pipeline, with survey candidates being migrated to pulsars.nanograv.org for inspection by high-school and undergraduate students (McLaughlin et al. 2023). To date, our survey has yielded 95 pulsar discoveries in total, including the ones we report in this work (see Table 1). Out of those, 14 are MSPs (Deneva et al. 2013; Martinez et al. 2017, 2019; Lewis et al. 2023) and 19 are so-called RRATs, only detectable through single pulses (Deneva et al. 2013, 2016). The survey is also sensitive to emission from known pulsars and we actively maintain a catalog³ of those detections (Deneva et al. 2024). These observations are valuable for studying pulse profile evolution, emission behaviors, scintillation, and other science. In the course of the survey, we have also developed two novel classifiers for single-pulse candidates, CLUSTER-RANK⁴ (Deneva et al. 2016) and SPEGID⁵ (Pang et al. 2018).

In addition to facilitating studies of emission behaviors, dedicated follow-up observations for a year or more allow the determination of timing solutions which constrain astrometric and spin-down parameters. In this paper, we present new pulsar discoveries, timing solutions for both new and previously published discoveries, and a brief census of emission properties for 49 pulsars

² <http://zmtt.bao.ac.cn/GPPS/GPPSnewPSR.html>

³ <http://ao327.nanograv.org/>

⁴ <https://github.com/juliadeneva/clusterrank>

⁵ <https://github.com/dipangwvu/SPEGID>

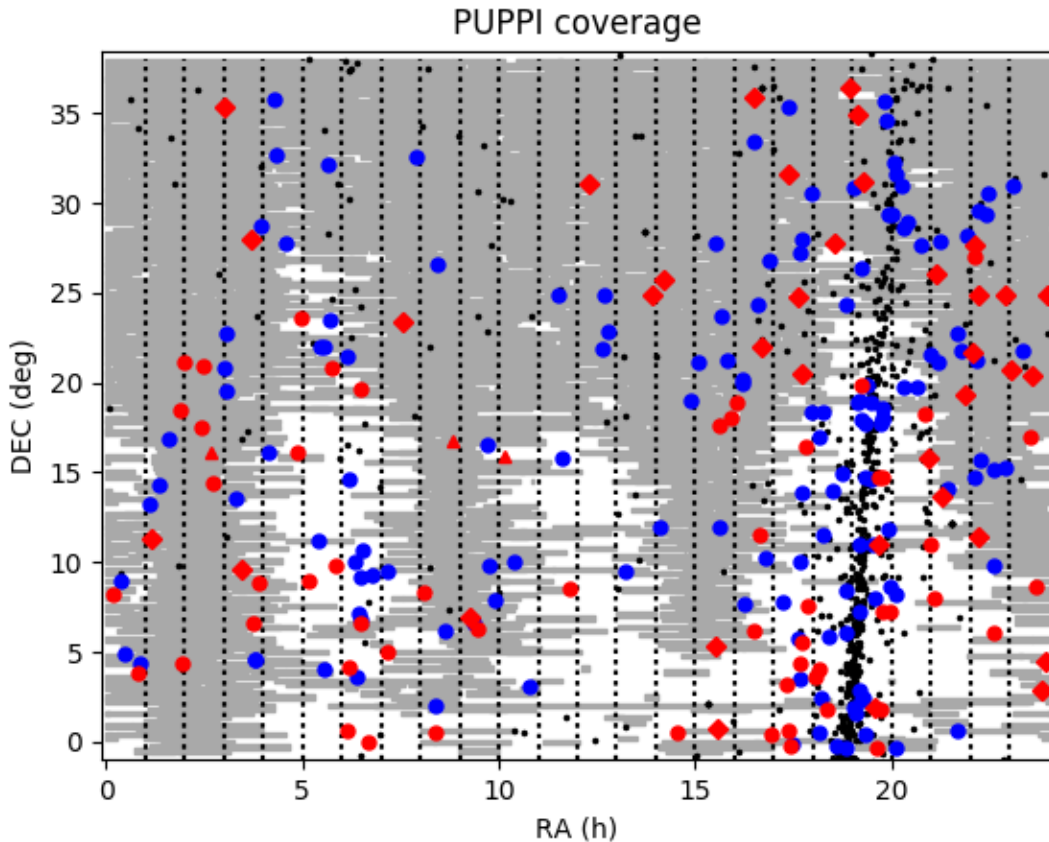


Figure 1. Both known and AO327-discovered pulsars in the sky visible from Arecibo. Grey strips indicate sky observed using the PUPPI backend. Black dots correspond to known pulsars from the ATNF catalog. Blue circles show known pulsars detected by the AO327 search pipeline. Red triangles indicate pulsars discovered using the WAPP backend, while red circles and red diamonds were found using the Mock and PUPPI backends.

discovered in the AO327 survey. Of these, 31 pulsars have already been published, while 18 are new discoveries. One of the 49 pulsars is a partially recycled pulsar. These pulsars were observed between the periods of 2013 – 2019 primarily using AO’s 327-MHz and L-band receivers. In §2 we describe our observations, §2.2 describes our survey’s search pipeline, §3 details our procedure for timing, §4 describes our results, and §5 gives a brief discussion of our results and conclusions.

2. OBSERVATIONS

2.1. Survey Observations

All sources presented in this paper were discovered with drift-scan observations at a center frequency of 327 MHz. The full width at half maximum power beam size of the Arecibo telescope at this frequency is $15'$, giving an approximate source transit time of about 1 minute. Raw total intensity data was taken and recorded using the “incoherent search mode” of the Puerto Rico Ultimate Pulsar Processing Instrument (PUPPI) back-

end at a sampling time of $81.92 \mu\text{s}$. The observations were configured to use 2816 frequency channels across the 68.75-MHz effective bandwidth of the 327-MHz receiver. Each full drift-scan observation was stored in a 4-bit format following the PSRFITS convention⁶. A catalog of the survey’s discoveries is kept on our webpage⁷.

2.2. Search Pipeline

Discoveries were made using our PRESTO⁸-based search pipeline (Ransom et al. 2002; Andersen & Ransom 2018; Ransom 2011). Search observations were first divided into 60-sec intervals with a stride of 30 sec (i.e., each interval overlaps by 30 sec of the adjacent interval) so as to ensure full coverage of sources transiting across

⁶ https://www.atnf.csiro.au/research/pulsar/psrfits_definition/Psrfits.html

⁷ <http://ao327.nanograv.org/newpulsars/>. For more details regarding the survey design, please refer to Deneva et al. (2013)

⁸ <https://github.com/scottransom/presto>

the telescope beam. The search pipeline was then deployed on each 60-sec interval. Using the PRESTO routine, `rfifind`, radio frequency interference (RFI) mitigation was performed by inspecting time chunks of ~ 2 seconds and flagging outlier time and frequency chunks corrupted by RFI. For more details of `rfifind` functionality, we refer the reader to Lazarus et al. (2015).

After RFI mitigation, the next steps are to remove the effects of dispersion by ionized gas along the line of sight (“dedispersion”) by summing the time series over all frequency channels, shifting each by the time needed to correct for dispersion delay, so as to maximize signal strength in the time domain. Interstellar dispersion is well-studied and imparts a frequency-dependent delay of

$$\Delta t = t_2 - t_1 = 4.15 \times \text{DM} \times (\nu_1^{-2} - \nu_2^{-2}) \quad (1)$$

where DM is the dispersion measure, or the integrated column density of free electrons along the line of sight, in units of pc cm^{-3} , ν_1 and ν_2 are the center frequencies of two channels given in GHz, and the delay between the arrival times in two channels Δt is measured in ms. Our maximum DM is set to correspond to a dispersion delay equal to the transit time of a source through the 327-MHz beam, while the DM step size is optimized based on the observing frequency, bandwidth and sampling time. We use the PRESTO routine `DDPlan.py` to compute the dedispersion plan as well as appropriate downsampling. Dedispersion was then performed utilizing `prepsubband` with downsampling factors of 1, 2, 4, and 8. Our maximum DM of $1438.2 \text{ pc cm}^{-3}$ is much higher than the expected Galactic contributions along all of the lines of sight sampled in our survey, providing good sensitivity to extragalactic FRBs.

There are two standard approaches for identifying astrophysical sources in dedispersed time series. The first uses Fourier analyses to detect periodic signals. These include the Fast Fourier Transform aided by harmonic stacking, and acceleration searches to increase sensitivity to binary pulsars (Ransom 2001). The apparent spin periods of pulsars in binary systems will vary due to Doppler shifts from binary accelerations. The degree of acceleration can be captured using parameter z , the Fourier frequency derivative that is induced by the observed variation in the rotational period. Standard convention is to define z in units of frequency bins drifted per observation length. We perform both low acceleration searches ($z_{max} = 0$), and high acceleration searches ($z_{max} = 50$). Harmonic summing was performed up to harmonics of order 16 (8) in our low (high) acceleration

searches. We then used `ACCELSift.py`⁹ to filter out spurious candidates caused by RFI or degeneracies in the Fourier search space. Candidates were then posted to the Pulsar Science Collaboratory pulsar searching website¹⁰ for visual candidate inspection (McLaughlin et al. 2023).

The second method is geared towards astrophysical sources that either are non-periodic or do not exhibit easily identifiable periodicity in their emission. Single-pulse searches (Cordes & McLaughlin 2003) exploit the dependence of signal-to-noise that an astrophysical pulse exhibits in the time vs DM parameter space. For each trial DM, downsampling is applied through convolution of a boxcar function so as to maximize signal to noise of any candidate single pulses. We perform a single-pulse search with PRESTO’s `single_pulse_search.py` using boxcar widths ranging from 1 up to 30 samples with the maximum pulse width not exceeding 0.1 s in length and choosing candidate pulses with a signal-to-noise ratio of 5.5σ or higher to be flagged for further inspection. We then applied two separate classifiers, CLUSTERRANK and SPEGLID, to filter out the best single-pulse candidates.

2.3. Timing Observations

Following discovery, a timing campaign was undertaken using AO’s 327-MHz and L-band receivers. Primary observations utilized the 327-MHz receiver in conjunction with the PUPPI backend. Observations varied in length, with a minimum integration time of 100 seconds in order to ensure a stable integrated profile. For each source, roughly half of the timing observations were taken in PUPPI’s coherent search mode and the remaining in coherent fold mode. The coherent modes perform coherent dedispersion, which more accurately removes the effects of interstellar dispersion compared to incoherent dedispersion (Hankins 2018), and search mode allowed for at least half of the observations for each source to have detectable single-pulses. Discovery dispersion measures (DMs – see Sec 2.2 for details) and the drift-scan backend configurations were used for these initial observations. We used 128 channels in coherent search mode. Once a satisfactory preliminary timing solution was found, we then used PUPPI’s coherent fold mode configured for full Stokes with 56 to 256 frequency channels. Sub-integration lengths of ~ 10.5 seconds were used for all sources except for J0916+0658. Sub-integration lengths must be shorter than the time it takes for profile drift caused by an incorrect folding

⁹ A description of the code can be found in Section 3.3.4 of Lazarus et al. (2015).

¹⁰ pulsars.nanograv.org

period to become significant, which roughly scales with a pulsar’s period. As J0916+0658 has a period of ~ 45 ms, we used a sub-integration length of ~ 2.5 seconds. Calibration data taken before each fold-mode observation consisted of an injection of a 25-Hz linearly polarized signal using a noise diode. Calibrator observations were 60 seconds, where 50% of this time had the noise diode engaged. Observations were taken over an approximately six-year period. Generally, several observations were taken at daily cadence, with the rest roughly split between weekly and monthly cadences depending on availability.

Observations using the L-band receiver were conducted for a subset of the 49 pulsars in conjunction with the PUPPI backend. All L-band observations were taken using PUPPI’s coherent search mode using a center frequency of 1380 MHz, a sampling time of 40.96 μ s, and 2048 frequency channels across the 800-MHz effective bandwidth. After coherent dedispersion within each of the 2048 channels, the frequency resolution was decimated to 128 channels. We first conducted a single observation of each source to estimate its L-band signal-to-noise. Bright sources were prioritized for further observations, while weaker sources were observed no more than a few epochs. We carried out no follow-up observations for non-detected sources.

3. ANALYSIS

After we confirm the discovery of a pulsar, we carry out a dedicated follow-up campaign (see Sec 2.3) to obtain its phase-connected timing solution. The data is also used to estimate some of their useful physical parameters such as characteristic age and inferred surface magnetic field strength (Lorimer & Kramer 2004). The details of these analyses are given below.

3.1. Timing Analysis

A time of arrival (TOA) is the absolute time at which a pulse is detected as measured at the observatory. We formed period-averaged profiles for each epoch of data using 256 bins, and measured TOAs by convolving this profile with a high signal-to-noise template profile. To create templates, we first excluded observations where RFI was egregious or the S/N was too low. We then selected an arbitrary epoch to serve as the reference profile and made use of the ‘Fourier-gradient method’ (Taylor 1992) to phase align each epoch’s profile with the reference profile. The phase offset between each individual and reference profile was computed by taking the Fourier transform of both and performing a cross-correlation. All profiles were then averaged to form an epoch-averaged profile of 256 bins. These are shown

in Figs. 6 – 10. The epoch-averaged profiles were then used as our templates for timing at 327 MHz. Given the spectra of these pulsars, noise-free templates were only produced at L-band. For L-band observations, we utilized noise-free Gaussian templates to reduce uncertainty in our TOA measurements.

To measure TOAs, for most observations we divided the complete observation into two subintegrations and two subbands, resulting in four TOAs per observation. For observations in coherent search mode, we used the PRESTO routine `get_TOAs.py` while those in fold mode we used PSRCHIVE’s `pat`. For each TOA, we measure a corresponding uncertainty in the arrival time.

TEMPO2 (Edwards et al. 2006) was utilized to construct the timing solutions, and unless otherwise noted, we use its default configuration and conventions. This code first converts TOAs from observatory topocentric time to Barycentric Coordinate Time (TCB) with the use of JPL’s DE436 ephemeris (Dai et al. 2024; Folkner et al. 2014). We fit the TOAs to a timing model accounting for spin period, period derivative, position, and dispersion measure through least-squares minimization of the residuals, or the differences between the measured and timing model-predicted TOAs. Depending on the complexity of the model, a parameter is added, and the process is reiterated for the remaining number of parameters, until all TOAs are phase-connected with low co-variances in the model parameters or relatively flat residuals on long time-scales. Because the uncertainties in the TOAs influence the uncertainties of parameters in the timing model, it is important to ensure that the errors on timing model parameters are not underestimated (Verbiest et al. 2016). It is convention to assume that the true uncertainty for a given TOA (σ_{new}) is simply proportional to its measured value (σ_{old}), $\sigma_{new} = F\sigma_{old}$, where the system-dependent constant of proportionality, F , is usually referred to as the EFAC. We then assume that the model is a perfect fit to the data and we scale the uncertainty such that $\chi^2_{\mu} = 1$ which corresponds to EFAC=1.

For all pulsars, we were able to construct phase-connected solutions using only basic astrometric and spin parameters and DM. PUPPI’s coherent search and coherent fold modes have different clock offsets, resulting in an intrinsic offset between the two groups of TOAs. We accounted for this by fitting a phase jump in the timing model when appropriate. Table 2 lists the fitted parameters as well as their associated errors. All solutions result in weighted root-mean-square residuals less than 0.3% of their spin periods. Furthermore, they also result in errors of less than 1% in their frequency

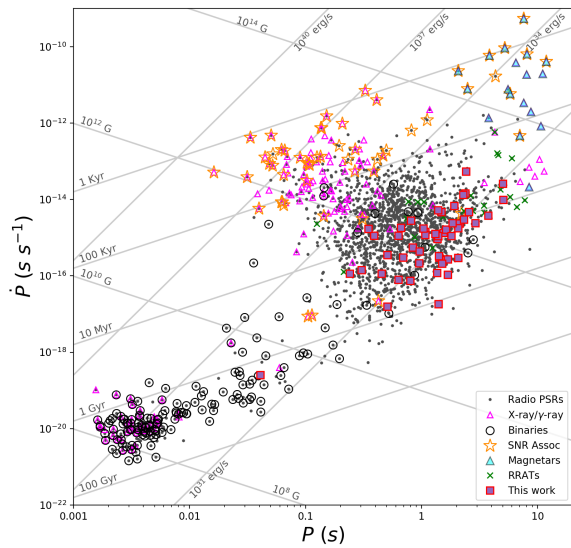


Figure 2. P- \dot{P} diagram showing the periods and period derivatives of known neutron stars. Black dots denote radio pulsars, purple diamonds X-ray/ γ -ray pulsars, black circles systems with companion objects, yellow stars sources with an associated supernova remnant, blue diamonds magnetars, green X's RRATs, and purple filled squares the pulsars included in this work. Also plotted are lines of constant \dot{E} , inferred magnetic field B , and characteristic age τ . The lower left population comprises the recycled population, while the center population comprises non-recycled pulsars. We note that the longest period pulsars lie to the upper right of the population corresponding to higher magnetic fields while the middle and shortest period pulsars show a broader variation in characteristic ages and \dot{E} 's.

derivatives. All solutions are adjusted to a reference epoch corresponding to the center of our data-span.

3.2. Flux Measurements

Flux densities were estimated from search mode observations through use of the radiometer equation¹¹. To account for the variable sky temperature, we followed the procedure outlined in Deneva et al. (2024) to estimate temperatures at 327 MHz. For the 327 MHz receiver, the system temperature was well-controlled and measured daily, with an average $T_{rec} = 113$ K. Prior to hurricane Maria's landfall on MJD 58012, the gain for the 327-MHz receiver was approximately 10 K/Jy, while after, the gain dropped to 8 K/Jy.

L-band observations were taken before hurricane Maria. The mean gain of the L-band receiver was

around 10.3 K/Jy while the system temperature was approximately 33 K. Estimation of the L-band sky temperature were made using the map available from the LAB HI survey (Kalberla et al. 2005; Land & Slosar 2007).

A flux density was estimated for each epoch and epoch-averaged flux densities are reported in Table 2 along with standard deviations.

3.3. Distance Measurements

Distances were estimated using DM measurements using the python package PyGEDM (Price et al. 2021) both for the NE2001 (Cordes & Lazio 2002) and YMW2016 (Yao et al. 2017) Galactic electron distribution models. The distances are reported in Table 2. Healpy (Zonca et al. 2019; Górski et al. 2005), the python implementation of HEALPix¹², was used for plotting purposes. A comparison of the two models predictions is shown in the top of Fig. 5 while the bottom shows sources with DMs exceeding one or both models maximum DM.

4. RESULTS

We present the first phase-connected timing solutions for 49 pulsars discovered in the AO327 survey. Of these, 18 are new discoveries. All but one of our sources appear to be non-recycled, or slow, pulsars.

4.1. Timing Results

Timing residuals for each source are shown in the Appendix. Each timing solution includes constraints on basic astrometric and spin parameters. In most cases, we have updated the source names based on better localization via timing as described in Table 1. Source periods and period derivatives are compared to other populations in Fig. 2. The spin periods of our pulsars range from 40 ms to 5.05 s, and their DMs from 17.8 pc cm⁻³ to 133.2 pc cm⁻³. As evident in Fig. 2, we find that the majority of our discoveries clearly skew towards older characteristic ages. This is consistent with other pulsar surveys from Arecibo (Parent et al. 2022), and low-frequency surveys such as LOFAR (Sanidas, S. et al. 2019) and LOTASS Michilli et al. (2019).

4.1.1. PSR J0916+0658

PSR J0916+0658 is an isolated pulsar with a period of 40.7 ms, and inferred surface magnetic field strength of 3.2×10^9 G. We find no evidence of accelerations indicating a companion, suggesting that J0916+0658 is a partially recycled pulsar.

¹¹ Using Equation 3 from Deneva et al. (2024)

¹² healpix.sourceforge.net

PSR (J2000)	R.A. (J2000) (h:m:s)	Dec. (J2000) (d:m:s)	ν (Hz)	$\dot{\nu}$ (Hz s^{-1})	DM (pc cm^{-3})	Epoch (MJD)	NT_{OAs}	RMS (μs)	χ^2	Data Span (Yr)	MJD Range (MJD)	$\log(\tau)$	$\log(B_{\text{surf}})$ (G)	$\log(\dot{E})$ (erg s^{-1})	D_{ne2001} (kpc)	D_{gmw16} (kpc)	$S_p \pm \sigma_{S_p}$ (mJy)	$S_l \pm \sigma_{S_l}$ (mJy)	EFs	
J0011+0845	00:11:42.32(3)	+08:05:42.62(10)	0.3917159530882(20)	-7.2027(12)E-16	24.758(13)	57808	81	823	3.0	5.1	56876-58740	6.9	12.5	31.0	1.3	5.0	0.3 \pm 0.1		AM, M?, N	
J0050+0248	00:50:22.80(15)	+03:47:58(3)	0.7317672555072(20)	-5.005(4)E-16	26.42(3)	57808	48	797	2.0	4.3	57203-58771	7.4	12.1	31.2	0.4	25.0	0.4 \pm 0.3		S	
J0158+2106	01:58:45.984(11)	+21:06:47(5)	1.97960408151(17)	-1.37960(4)E-15	19.777(12)	57815	160	930	3.8	5.6	56494-58532	7.4	11.6	32.0	1.9	1.5	0.7 \pm 0.3	0.31		S
J0225+1227	02:25:22.288(11)	+17:27:44.1(5)	2.56275725492(12)	-7.44343(14)E-15	19.975(6)	57846	128	288	1.6	5.0	56641-58451	6.7	11.8	32.9	0.8	1.4	0.8 \pm 0.4	0.17		IP, S
J0229+2058	02:29:11.995(9)	+20:58:34.3(4)	1.239438282432(5)	-4.31612(20)E-15	26.664(6)	57475	135	486	2.6	5.3	56500-58445	6.7	12.2	32.3	0.8	2.0	0.3 \pm 0.5	0.03 \pm 0.02	$D_1^?$, M?, N, S	
J0241+1604	02:41:25.79(8)	+16:04:14(4)	0.647265962072(8)	-5.60985(20)E-16	19.558(7)	57821	140	377	1.0	6.2	56495-58744	7.3	12.2	31.2	1.3	1.3	0.6 \pm 0.2			AM
J0245+1433	02:45:19.89(6)	+14:33:19(3)	0.4699401903062(13)	-5.2125(3)E-16	29.506(9)	57821	86	598	5.4	6.2	56499-58744	7.2	12.4	31.0	1.2	2.5	1.0 \pm 0.5			AM, N
J0457+2333	04:57:03.00(2)	+23:33:52(3)	1.980583294463(4)	-6.1170(6)E-17	58.472(7)	57816	48	237	2.5	5.1	56890-58744	8.7	11.0	30.7	1.9	1.5	2.0 \pm 0.4			AM, N
J0608+0044	06:08:48.540(3)	+00:44:11.06(8)	0.929218888961(6)	-1.2149(5)E-15	48.434(2)	56898	82	318	3.4	2.0	56532-57258	7.1	12.1	31.6	1.9	1.3	1.5 \pm 0.6	0.13 \pm 0.12		D
J0611+0411	06:11:51.800(18)	+04:11:09.8(3)	0.597211849968(19)	-3.415(3)E-17	69.63(3)	57308	47	867	1.0	2.2	56916-57701	8.4	11.6	30.0	2.6	1.7	0.2 \pm 0.1			AM, D, N
J0627+0049	06:27:53.6275(7)	+06:49:54.06(4)	2.885811444479(3)	-1.41456(1)E-14	86.512(4)	57325	116	144	2.1	4.5	56500-58152	6.5	11.9	33.2	1.8	1.9	1.9 \pm 1.8	0.06 \pm 0.06		AM
J0639-0004	06:39:44.592(14)	-00:04:53.4(3)	0.41500946624(9)	-9.2020(10)E-16	70.09(4)	56950	75	1233	0.8	2.2	56554-57347	5.8	13.1	32.2	2.5	1.8	0.4 \pm 0.2			AM, N
J0806+0811	08:06:18.629(7)	+08:11:54.8(4)	0.484706686755(6)	-6.968(12)E-17	46.700(16)	57396	150	930	3.2	4.9	56500-58293	8.0	11.9	30.1	2.0	1.9	0.6 \pm 0.2	0.42		AM, M, N
J0848+1604	08:48:44.016(9)	+16:40:24.6(5)	2.210647285054(14)	-5.6118(3)E-16	38.556(20)	57366	152	112	1.1	4.8	56500-58234	7.8	11.4	31.7	1.8	2.4	0.6 \pm 0.2	0.04 \pm 0.03	AM, D?, M, N	
J0916+0658	09:16:15.2394(17)	+06:58:32.89(9)	24.5142854050(9)	-4.152(6)E-16	19.1720(16)	58210	116	99	4.6	1.4	57957-58463	9.4	9.5	32.2	0.7	0.9	1.8 \pm 0.8			AM, D, N
J0928+0014	09:28:29.908(3)	+06:14:08.44(10)	0.485378446936(16)	-4.21575(12)E-16	50.480(5)	57481	194	270	1.7	5.4	56500-58463	7.3	12.3	30.9	41.0	25.0	0.8 \pm 0.3			AM
J1147+0829	11:47:42.756(19)	+08:29:04.0(7)	0.615361380485(4)	-6.158(3)E-16	26.595(16)	57644	113	851	1.4	3.3	57049-58240	7.2	12.2	31.2	1.6	25.0	0.2 \pm 0.1	0.11 \pm 0.07		N
J1215+3058	12:15:58.977(8)	+30:58:45.97(19)	1.196223322341(15)	-7.87(3)E-16	15.557(9)	57999	60	362	1.3	1.1	57789-58210	7.4	11.8	31.6	1.3	1.9	0.3 \pm 0.2			AM, N, S
J1531+0519	15:31:40.35(3)	+05:19:49.3(6)	0.7042133869107(19)	-1.50(4)E-16	31.27(7)	58444	63	2089	1.3	1.6	58155-58734	7.9	11.8	30.6	3.1	25.0	0.3 \pm 0.2			AM, M, N
J1538+1736	15:38:10.473(4)	+17:36:10.24(8)	1.448665690319(6)	-6.331(3)E-16	34.588(13)	57446	158	904	3.8	4.2	56936-58477	7.6	11.7	31.6	32.4	25.0	0.3 \pm 0.2	0.10 \pm 0.05		AM, M
J1628+0613	16:28:53.936(5)	+06:13:54.60(14)	0.723782796197(3)	-5.8216(10)E-16	51.701(7)	57485	125	697	1.1	4.6	56647-58525	7.3	12.1	31.2	44.2	25.0	0.4 \pm 0.2	0.22 \pm 0.05		AM, M
J1637+0013	16:37:47.6875(14)	+11:31:59.39(4)	0.598766594449(10)	-2.8175(4)E-17	53.913(4)	57485	124	280	1.2	4.6	56647-58525	8.1	11.8	30.4	43.8	25.0	1.2 \pm 0.5	0.69		AM, D, N
J1656+0018	16:56:31.830(19)	+00:18:04.4(4)	0.667584921012(10)	-9.39(4)E-17	47.42(3)	57685	81	1742	2.8	4.3	56894-58747	8.1	11.8	30.4	2.1	4.0	0.3 \pm 0.2			AM, N, S
J1726-0022	17:26:27.278(12)	-00:22:00.8(3)	0.764752927739(13)	-7.300(8)E-16	59.857(18)	57104	68	869	1.2	2.5	56647-57562	7.2	12.1	31.3	2.2	3.3	0.4 \pm 0.1			AM, N, S
J1738+0418	17:38:24.575(3)	+04:18:15.25(10)	0.71855689349(19)	-9.5(3)E-18	55.432(16)	57323	71	339	2.6	2.0	56963-57884	9.1	11.2	29.4	1.1	1.1	0.5 \pm 0.1			AM, N
J1743+0532	17:43:04.452(12)	+05:32:11.34(15)	0.6785589822200(10)	-2.157(3)E-15	59.50(4)	57450	64	622	0.8	1.3	57218-57084	6.7	12.4	31.8	3.1	3.9	1.1 \pm 0.3			AM?
J1749+1629	17:49:10.45(3)	+16:29:43.0(5)	0.4327133602497(14)	-5.55(5)E-16	59.50(4)	57450	43	1694	1.3	1.3	57231-57712	7.1	12.4	31.0	3.1	7.5	0.3 \pm 0.2			AM, N
J1802+0733	18:02:38.258(3)	+03:59:29.26(5)	1.251928081695(8)	-1.1578(19)E-16	52.694(5)	57029	100	280	1.0	2.9	56496-57562	8.2	11.4	30.8	2.0	2.4	1.2 \pm 0.6	0.22		AM
J1807+0359	18:07:15.858(3)	+03:59:29.26(5)	1.583013056092(9)	-2.2157(5)E-15	94.19(4)	58049	98	186	1.8	4.6	57110-58772	6.9	11.9	32.2	2.7	3.9	0.8 \pm 0.3			AM, D?
J1812-1947	18:12:51.077(12)	+19:47:40.38(15)	0.420841476666(7)	-2.542(3)E-15	94.19(4)	58049	71	1079	1.7	1.2	57826-58273	6.4	12.8	31.6	4.3	7.1	1.0 \pm 0.3			AM, D?, N
J1917+3115	19:17:33.045(4)	+31:15:05.65(6)	0.544273079951(15)	-7.0485(11)E-16	81.091(12)	58329	98	465	3.0	2.8	57826-58834	7.1	12.3	31.2	4.3	3.3	0.5 \pm 0.3			AM, D?
J1937-0023	19:37:02.3896(15)	-00:23:40.66(7)	4.163304873766(14)	-1.96(4)E-16	77.882(4)	57634	107	228	2.9	6.2	56496-58772	7.5	11.2	32.5	2.6	3.4	0.9 \pm 0.4	0.17 \pm 0.06		
J1938+1105	19:38:07.62(7)	+15:05:36.8(10)	0.344534883236(6)	-2.80(3)E-16	74.44(14)	57278	62	4878	2.4	1.2	57053-57504	7.3	12.4	30.6	3.5	2.6	0.5 \pm 0.4			D, N
J1942-0147	19:42:13.936(9)	+01:47:59.7(2)	0.711856908341(4)	-1.657(4)E-16	133.19(3)	57912	109	1081	2.3	4.7	57053-58772	7.8	11.8	30.7	5.6	3.6	1.7 \pm 1.0	0.22		D*, N
J1945+0720	19:45:44.833(3)	+07:20:40.75(7)	0.96738761540(3)	-1.086(5)E-16	47.38(1)	57634	104	402	7.9	6.2	56496-57504	7.2	12.1	31.6	2.8	2.6	0.5 \pm 0.2			AM?
J1946+1447	19:46:43.16(3)	+14:47:46.7(3)	0.43815067512(3)	-2.548(4)E-15	50.51(4)	57278	58	1247	1.4	1.2	57053-57504	6.4	12.8	31.6	2.8	2.8	1.5 \pm 0.2			AM, N
J1957+0724	19:57:03.85(3)	+07:24:24.5(4)	0.1994415276246(15)	-1.02122(13)E-15	61.76(5)	58011	73	1560	0.4	4.3	57231-58792	6.5	13.1	30.9	2.9	3.2	0.2 \pm 0.1			AM, N
J2050+1100	20:50:04.675(5)	+11:00:29.8(4)	1.048373857300(5)	-2.338(3)E-16	60.298(8)	57520	52	261	0.9	3.1	56948-58093	7.8	11.7	31.0	4.2	25.0	0.7 \pm 0.1			AM, D?, N
J2105+0757	21:05:26.193(19)	+07:57:57.9(0)	0.266917176516(3)	-2.675(4)E-16	52.48(5)	57667	86	1950	1.0	4.1	56917-58417	7.2	12.6	30.5	3.5	3.5	0.6 \pm 0.2			D, N
J2151+1918	21:51:11.459(10)	+19:18:12.54(15)	0.96738761540(3)	-1.6137(8)E-15	30.953(18)	58053	54	703	1.5	2.3	57638-58478	7.0	12.1	31.8	3.8	7.5	0.5 \pm 0.1			AM
J2202+2134	22:02:16.9853(19)	+21:34:33.88(6)	0.73621113315584(12)	-6.525(5)E-17	17.763(3)	58360	114	332	0.5	2.6	57888-58834	8.2	11.6	30.3	1.3	1.4	0.5 \pm 0.2			AM, N
J2252+2455	22:52:19.036(4)	+24:55:56.12(8)	0.5562001939124(19)	-3.457(3)E-16	34.788(13)	58506	86	447	2.2	1.8	58180-58834	7.4	12.2	30.9	3.9	4.0	0.5 \pm 0.1			D, N
J2329+1657	23:29:39.247(11)	+16:57:17.7(3)	1.582029754326(11)	-1.994(3)E-16	30.438(20)	57747	107	1028	1.0	5.5	56737-58758	8.1	11.4	31.1	1.8	7.1	0.3 \pm 0.1	0.19 \pm 0.09		AM, D?
J2340+0831	23:40:51.948(3)	+08:31:21.57(10)	3.297275696476(4)	-1.83789(3)E-15	23.777(3)	57412	147	271	3.5	5.8	56347-58478	7.5	11.3	32.3	3.2	3.2	2.1 \pm 1.4	0.10 \pm 0.03		AM, D?
J2347+0500	23:47:44.471(16)	+03:00:12.1(6)	0.72144716244018(11)	-2.75676(17)E-15	16.207(4)	58179	49	220	1.7	3.1	57618-58740	6.6	12.4	31.9	1.8	1.6	1.7 \pm 0.1			AM, N
J2354+0434	23:54:08.76(8)	+04:34:04(3)	1.0457545445235(10)	-4.785(13)E-16	12.58(3)	58160	91	1306	4.0	3.2	57580-58740	7.5	11.8	31.3	0.6	1.1	1.5 \pm 0.4			AM, N

Table 2. A0327 pulsar discoveries with completed timing solutions. Columns are as follows: (1) the pulsar name based on the timing-derived position, (2-3) the right ascension and declination, (4-5) the spin and spindown frequencies, (6) the DM, (7) the reference epoch used for the timing model, (8-9) the number of TOAs and weighted RMS of the residuals, (10) the chi-squared χ^2 of the timing residuals, (11-12) the total time span of the TOAs and the MJD range, (13-15) the characteristic age τ , inferred surface dipolar magnetic field B , and the spin-down energy loss rate \dot{E} , (16-17) distances derived from the NE2001 and YMW2016 electron density models, (18) average observed 327 MHz flux density and standard deviation, (19) average observed 1380 MHz flux density and standard deviation, and (20) the associated emission features. Numbers in the parentheses are the 1σ -uncertainties on the last digit as reported by TEMPO2, after weighting the TOAs such that reduced chi-squared $\chi^2_{\text{red}} = 1$. Flux uncertainties are only reported for cases where more than one detection was made. Emission features by alphabetical ordering are: (D) drifting, (D^*) bi-drifting, (IP) interpulse, (M) mode-changing, (N) nulling, (AM) amplitude modulation, (PC) postcursor, (S) scintillation. In some cases, it remained difficult to make a clear identification of emission features. In such cases, we provide a best guess with a question mark.

Based on the criterion set forth by Belczynski et al. (2010), PSR J0916+0658 is a disrupted recycled pulsar (DRP). DRPs are believed to originate as the first-born neutron stars in high-mass binary systems, with accretion taking place between the pulsar and companion. Eventually, the companion undergoes a supernova explosion and imparts a kick on the system. When the kick is of sufficient strength to disrupt the binary, the recycled pulsar becomes isolated and therefore a DRP, while weak kicks that fail to disrupt the binary form double neutron star (DNS) systems. DRPs are very rare (Fiore et al. 2023; Swiggum et al. 2023; Belczynski et al. 2010). The DRPs and DNS populations share the same evolutionary channel, and so their populations each give better constraints on the formation processes. To date, 19 DNS systems are known, while the number of DRPs is around 20 (including J0916+0658). It is still unclear why there are not more DRPs as evolutionary models suggest DRPs should be several times more abundant than DNS systems. One suggested explanation is that neutron stars in close, interacting binaries receive much smaller natal kicks than other pulsar population models suggest (Belczynski et al. 2010).

4.2. Emission Features

In addition to constructing phase-connected timing solutions, our multi-epoch observations with single-pulse resolution provide us an opportunity to probe related emission behaviors for these sources. In total, 29 of our sources show some form of amplitude modulation alone, one source showing drift alone, and 13 showing evidence of both. In addition, PSR J1942+0147 was found to exhibit bi-drifting, a rare type of subpulse drift in which the drift slopes have different signs for different components. This is seen in only a handful of sources (Szary et al. 2020). An example of this pulsar’s bi-drifting is shown in Fig. 3, while an example of mode changing behavior by PSR J0806+0811 is shown in Fig. 4. Documented emission features are listed in Table 2. In cases where identification was uncertain, entries are marked with a question mark. A detailed study of the pulsars emission features will be left to forthcoming work. The 327-MHz epoch-averaged intensity profiles for each pulsar are shown in Figs. 6–9 while L-band profiles are shown in Figs. 11–12. Also, we note that one pulsar, PSR J0225+1727, with spin period of 390 ms, has an interpulse offset by 164° from the main pulse. Though the main-pulse of J0225+1727 was weakly detected at L-band, no detection of the interpulse was made.

4.3. Distances

The DM-derived distances for most sources generally agree between the two electron density models NE2001

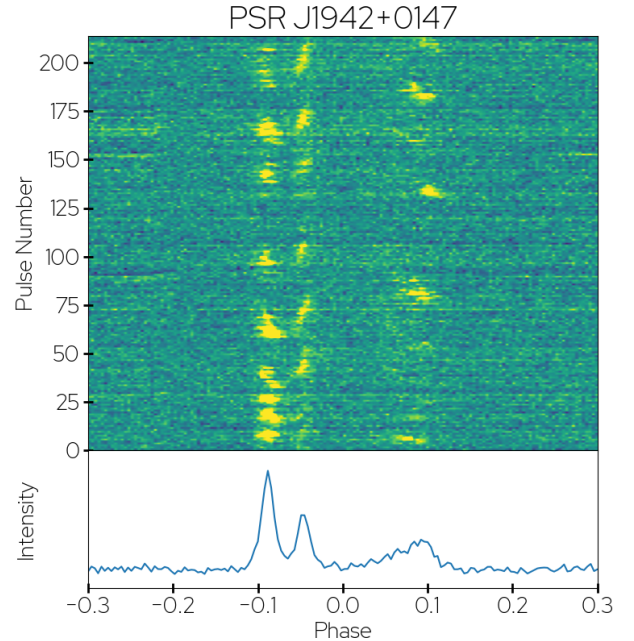


Figure 3. Top: Pulse sequence for bi-drifting PSR J1942+0147. Below: The epoch-averaged intensity profile over 60% of the full pulse profile. Note the change in drift direction over the components. This pulsar has a rather broad profile for its spin parameters, comprising four-components as inferred from its epoch-averaged profile. Four-component profiles are believed to be associated with unusual viewing geometries (Rankin 1993; Teixeira et al. 2015). The bi-drifting further supports this conclusion.

and YMW2016 (see Table 2) as shown in the top of Fig. 5. In general, distance estimates from density models can show significant differences from true, or parallax-inferred, distances. Price et al. (2021) found that for 57 parallaxes measured from the PSR π survey, 86% of NE2001 distance estimates ranged from $0.12\text{--}4.10 \times D_{\text{measured}}$ while 82% of YMW16 distance estimates ranged from $0.22\text{--}3.33 \times D_{\text{measured}}$, where D_{measured} is the distance inferred from parallax. It is important to note, that the number of parallax measurements is not many, the model errors are heavily direction-dependent, and the majority of our sources are in parts of the sky undersampled by the PSR π survey as well as other surveys. However, we can explore if our sources are consistent with these limits. Based on the previous values, we can infer that $\sim 80\%$ of sources should see $-1.44 < \log_{10}(\frac{D_{\text{ymw16}}}{D_{\text{ne2001}}}) < 1.27$. As can be seen in Fig. 5, only five sources exceed these limits. This is consistent given the size of our sample.

In general, we find that for most of our sources, the distance estimates from the two models are within a factor of two or three of each other. A few sources with

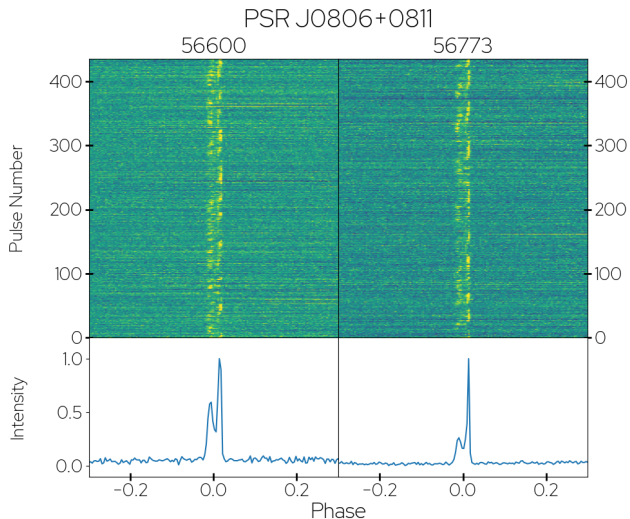


Figure 4. Mode-changing PSR J0806+0811 observed at 327 MHz. Top: Pulse number vs pulse phase, with color representing intensity. Below: The average profile for this observation. The most significant difference between the two modes can be seen from the relative intensity of the two components. The leading component appearing more often in single pulses on MJD 56600 resulting in a brighter component.

discrepant distance estimates are close to known pulsars for which model distance estimates agree. For example, PSR J1942+0147, for which the two distance estimates are very discrepant (25 kpc using YMW16 and 5.6 kpc with NE2001), is only 0.5 degrees away from J1941+0121, for which the distances estimates show excellent agreement (2.1 kpc using YMW16 and 2.2 kpc with NE2001). For PSR J0050+0348, another source with discrepant estimates (25 kpc in YMW16 and 1.4 kpc with NE2001), the nearest source PSR J0051+0423 is 0.64 degrees away and shows better agreement between the distance estimates (1.2 kpc using YMW16 model and 0.6 kpc with NE2001). For other sources, there is no other pulsar within a one degree radius.

We also explored model predicted maximum DMs in the directions of our source as shown in the bottom of Fig. 5. We identify 10 sources where the observed DM exceeds the predicted maximum from either YMW16 (10), or both NE2001 and YMW16 (4). Those sources are PSRs J0050+0348, J0928+0614, J1147+0829, J1531+0519, J1538+1736, J1628+0613, J1637+1131, J1942+0147, J2059+1100, and J2105+0757. These sources lie predominately off the galactic plane, and occupy lines of sight not previously sampled. The DM excesses for cases where only YMW16 fails are on average lower than those in cases where both models fail. The majority of the DM excesses occur at relatively high latitudes. The largest YMW16 excesses occur for northern

latitudes and correspond to cases where NE2001 also fails. For sources south of the Galactic equator, only YMW16 fails. While YMW16 was constructed using a larger sample of parallax measurements as compared to NE2001, YMW16 makes no effort to correct for DM excesses by inclusion of clumps or voids whereas NE2001 does. This may explain some of the differences in performance we see, though it is also clear that both models are insufficient to model electron densities along novel lines of sight.

5. DISCUSSION

Here we discuss some of the individual objects which show interesting emission phenomenology.

5.1. PSR J0225+1727

Pulsar emission is generally confined to a primary window of emission, or a so-called main pulse (MP), with typical duty cycle of a few percent. In rare cases, pulsars show interpulses (IPs), or secondary windows of emission offset from the main pulse by around 180° , though this can vary by up to $\sim 30^\circ$. IPs can arise either as a consequence of a double-pole (DP) emission geometry (Cady & Ritchings 1977), where the line of sight intersects emission from both magnetic poles or a one-pole emission geometry, in which both the MP and IP arise from the same magnetic pole due to a nearly aligned rotation and magnetic axis (Manchester & Lyne 1977). For at least some IPs, studies of polarization position angle (PPA) tracks strongly support a two-pole interpretation (Keith et al. 2010) while there are others where the polarization is unable to effectively distinguish between aligned and orthogonal geometries (Everett & Weisberg 2001). Polarization is key to determining the emission geometry, and we plan a careful study of this pulsar’s polarization in forthcoming work.

Maciesiak et al. (2011) and Belczynski et al. (2010) provide the most recent study of commonality of IP emission among the pulsar population. At the time of their writing, the number of known pulsars totaled around 1500 with $\sim 2\%$ exhibiting IPs. This is roughly consistent with a recent paper on FAST-discovered pulsars, in which 39 of the 682 pulsars have IPs (Wang et al. 2023). For a purely random distribution of alignments, $\sim 5\%$ of pulsars should exhibit IPs (Weltevrede & Johnston 2008), more than half of what is actually observed. Both Maciesiak et al. (2011) and Weltevrede & Johnston (2008) were able to reconcile this discrepancy under the condition that the magnetic axis undergoes alignment on >10 MYr time-scales, which would also explain the observed period distribution of pulsars with IPs (Weltevrede & Johnston 2008). More recently, Arzamasskiy

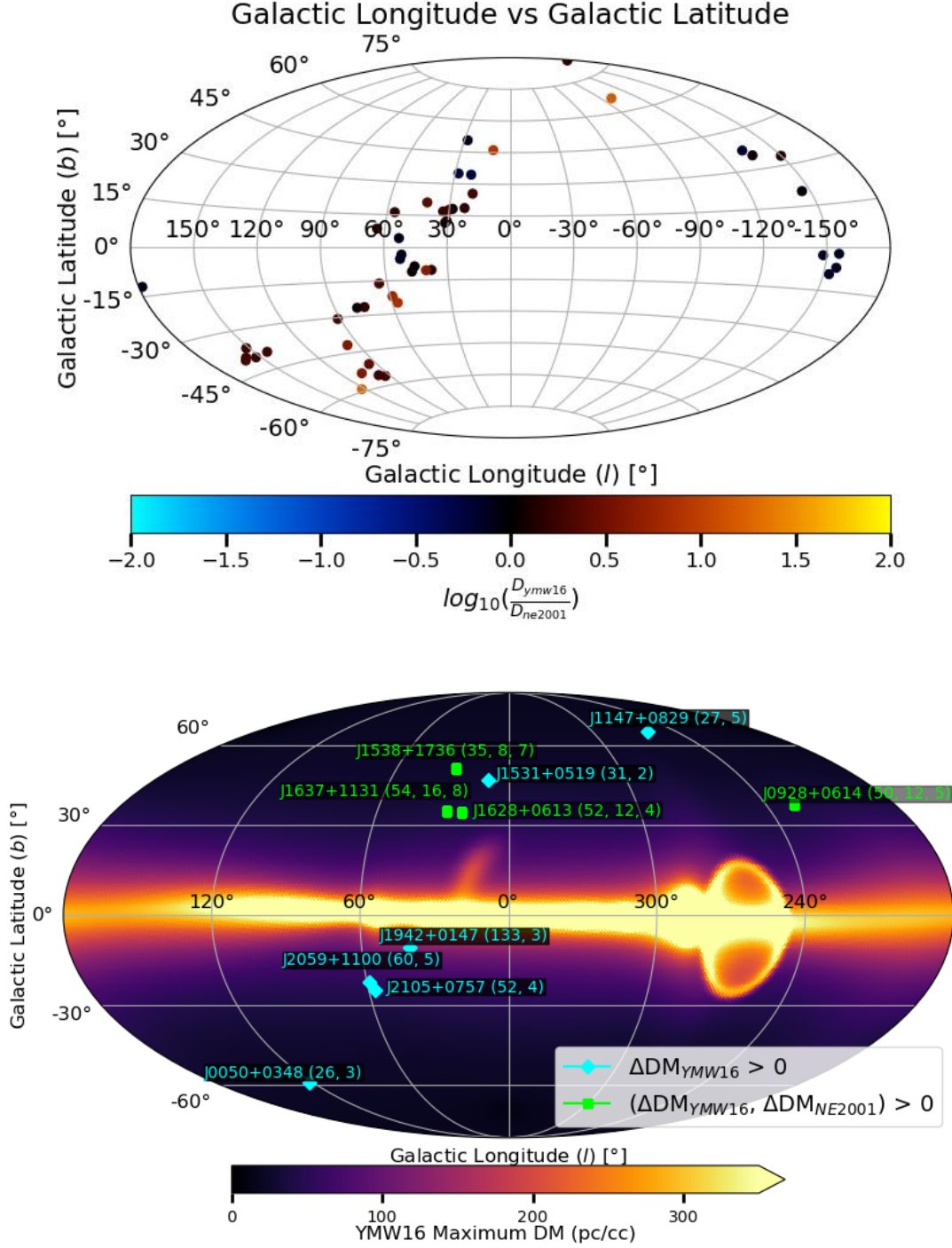


Figure 5. Top: All-sky map (Aitoff projection) showing the location of Table 2 sources and the log-ratio of predicted distances from YMW16 to NE2001. Model predictions show relative agreement for the majority of sources, though there are significant differences for several sources. Bottom: All-sky maps (Mollweide projection) in Galactic coordinates showing a continuous map of YMW16 predicted DMs for sources located at a distance of 30 kpc. Sources where observed DMs exceed the YMW16 predictions are labeled with teal diamonds while cases where DMs exceed both both models we label with green squares. Additionally we have plotted the name of each source followed in parentheses by source DM, and YMW16 and (where present) NE2001 DM excesses ($\Delta DM_{model} = DM_{obs} - DM_{model}$ ($d = 30$ kpc)). As all our sources lie on relatively low density lines of sight, for comparison purposes we have limited the color bar to a maximum DM of 350 pc cm^{-3} . In total, 10 sources exceed the YMW16 predictions, while four sources exceed both the NE2001 and YMW16 predictions. We note that a majority of the DM excesses are for sources out of the Galactic plane. We also note that the northern YMW16 excesses are also the largest and correspond to cases where both models fail.

et al. (2017) pointed out that counter-alignment was an equally viable explanation as well as predicting period dependencies of both cases for one and two-pole IPs. Determining the emission geometry for PSR J0225+1727 and other new IP pulsars are useful constraints for better determining how the magnetic axis evolves in time. With the recent doubling of IPs from FAST, theorists are well-positioned to improve model constraints. We note PSR J0225+1727 has an old dynamical age relative to other IP pulsars, as seen in Fig. 6 from Maciesiak et al. (2011), and may be an informative source depending on the statistics of IPs gleaned from FAST.

5.2. PSR J1942+0142

Nearly all pulsars that exhibit subpulse drift have a preferred drift direction over the entire profile. Only three pulsars – PSRs J0815+0939, J1034–3224, and B1839–04 – are known to show the phenomenon of bi-drifting (McLaughlin et al. 2004; Szary et al. 2020), in which the direction of subpulse drift can change between emission components. The bi-drifting of PSR J1942+0142 is shown in Fig. 3. This pulsar also has a rather wide four-component profile, with the later two merged, as evident from its epoch-averaged profile in Fig. 8. Similar to PSR J0815+0939, four-component profiles are indicative of an unusual emission viewing geometry (Rankin 1993).

The cause of subpulse drift is still debated. As described by van Leeuwen & Timokhin (2012), above the polar cap the electric potential should vary between adjacent field lines, giving rise to a tangential component of the electric field E_{\perp} . This then leads to an $\vec{E} \times \vec{B}$ of outflowing plasma, which traditionally¹³ has been favored as the cause of subpulse drift. In this picture, variation of electric potential across the polar cap can give rise to bi-drifting (van Leeuwen & Timokhin 2012). Szary & van Leeuwen (2017) expanded on this, and noted that in the presence of multipolar fields, the drift no longer centers around the magnetic axis, but instead around the polar cap potential minimum. Interestingly, this also leads to the semi-empirical model of Wright & Weltevrede (2016). What the physical implications of bi-drifting entail are still in its infancy, and with so few known sources in the literature, detailed cases studies are very important for improving constraints on emission models. We leave a detailed study of the drift to a forthcoming work.

6. CONCLUSION

We have presented complete timing solutions for 49 pulsar discoveries from the AO327 survey, including one partially recycled pulsar and 46 non-recycled pulsars. They skew towards large characteristic ages and lower DMs as expected for sources found in this type of survey.

We find 29 pulsars which show some form of amplitude modulation alone, one source showing drift alone, and 13 showing evidence of both. Among these sources, J1942+0147 exhibits the rare effect of bi-drifting, and J0225+1727 possesses an interpulse. Future studies will explore the emission features in this set of pulsars as well as their polarization properties.

In total, 95 pulsars have been discovered in the AO327 survey. These are the last of the AO327 discoveries which can be followed up with the Arecibo Observatory. Currently, less than 2% of survey search observations remain to be processed and more than 60% of search candidates remain to be inspected. We expect at least another 100 pulsars to be discovered, and their followup will necessitate other instruments, with the faintest sources requiring the use of the FAST telescope in China.

ACKNOWLEDGMENTS

M.A.M., E.F.L., and T.E.E.O. are supported by NSF award AST-2009425. J.S.D is supported by NSF award AST-2009335. M.A.M. is also supported by NSF Physics Frontiers Center award PHYS-2020265. This research was made possible by the NASA West Virginia Space Grant Consortium, Grant #80NSSC20M0055. The Arecibo Observatory was a facility of the National Science Foundation operated under co-operative agreement by the University of Central Florida and in alliance with Universidad Ana G. Mendez, and Yang Enterprises, Inc. Some of the results in this paper have been derived using the healpy and HEALPix package.

¹³ van Leeuwen & Timokhin (2012) include a review of alternate models which we refer the interested reader to.

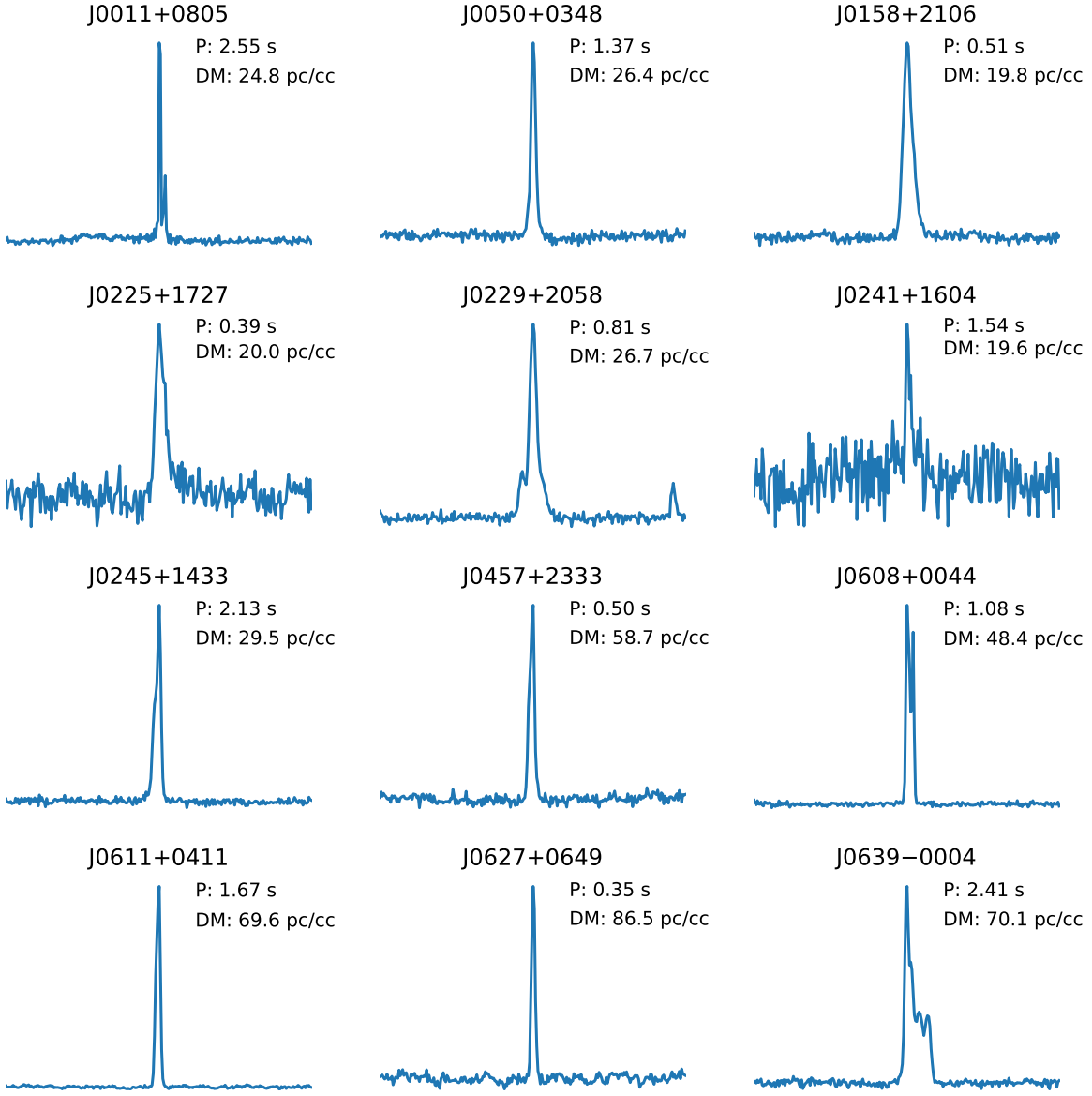


Figure 6. Epoch-averaged intensity profiles at 327 MHz. We plot intensity on the y-axis and rotational phase on the x-axis. One full rotation is shown. Each profile has a resolution of 256 phase bins. We label each profile with the pulsar's period and DM.

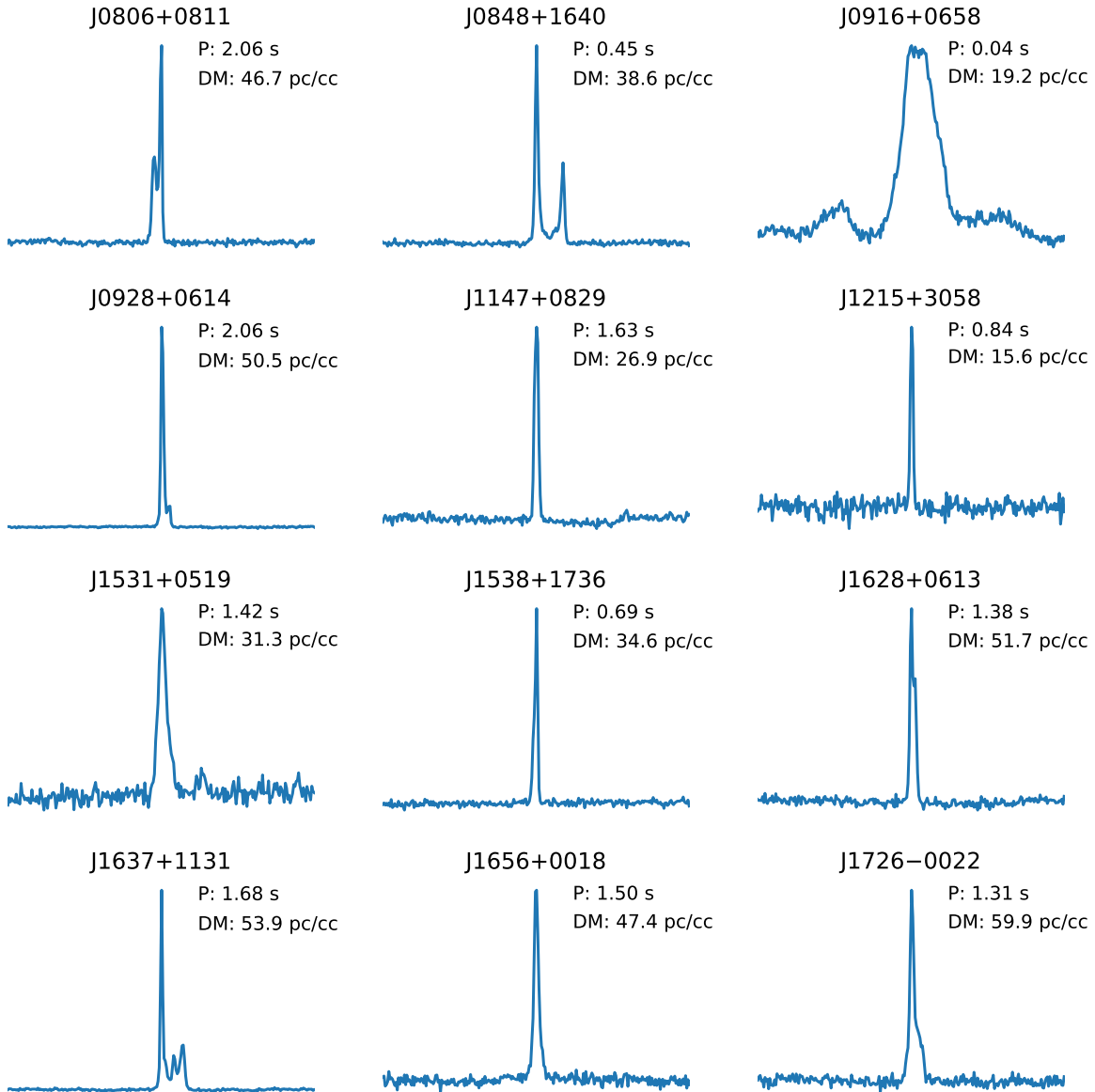


Figure 7. Epoch-averaged intensity profiles at 327 MHz. We plot intensity on the y-axis and rotational phase on the x-axis. One full rotation is shown. Each profile has a resolution of 256 phase bins. We label each profiles with the pulsar's period and DM.

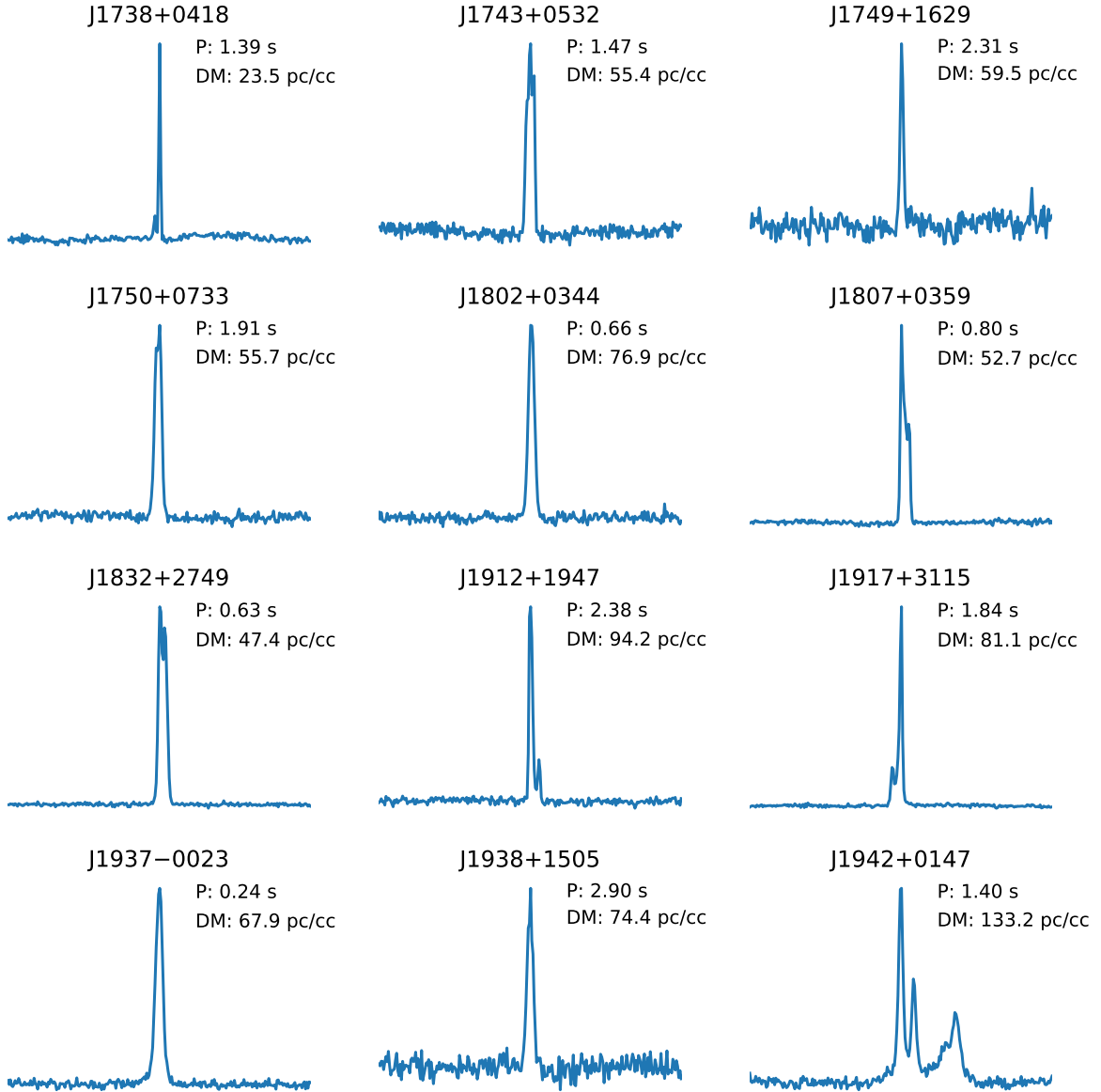


Figure 8. Epoch-averaged intensity profiles at 327 MHz. We plot intensity on the y-axis and rotational phase on the x-axis. One full rotation is shown. Each profile has a resolution of 256 phase bins. We label each profile with the pulsar's period and DM.

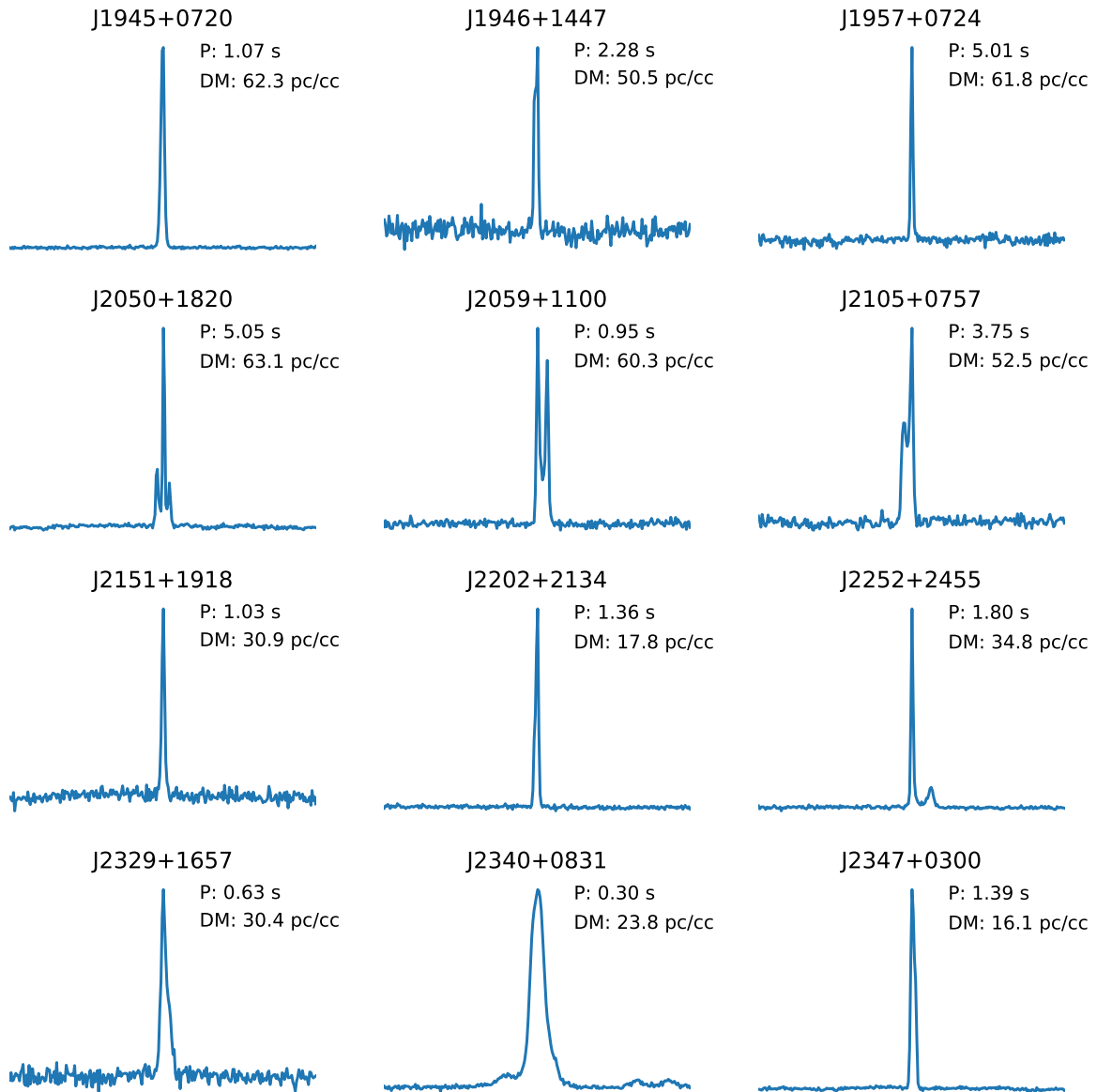


Figure 9. Epoch-averaged intensity profiles at 327 MHz. We plot intensity on the y-axis and rotational phase on the x-axis. One full rotation is shown. Each profile has a resolution of 256 phase bins. We label each profile with the pulsar's period and DM.

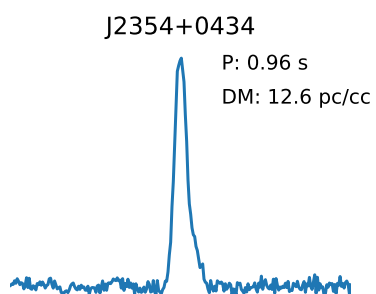


Figure 10. Epoch-averaged intensity profiles at 327 MHz. We plot intensity on the y -axis and rotational phase on the x -axis. One full rotation is shown. Each profile has a resolution of 256 phase bins. We label each profile with the pulsar's period and DM.

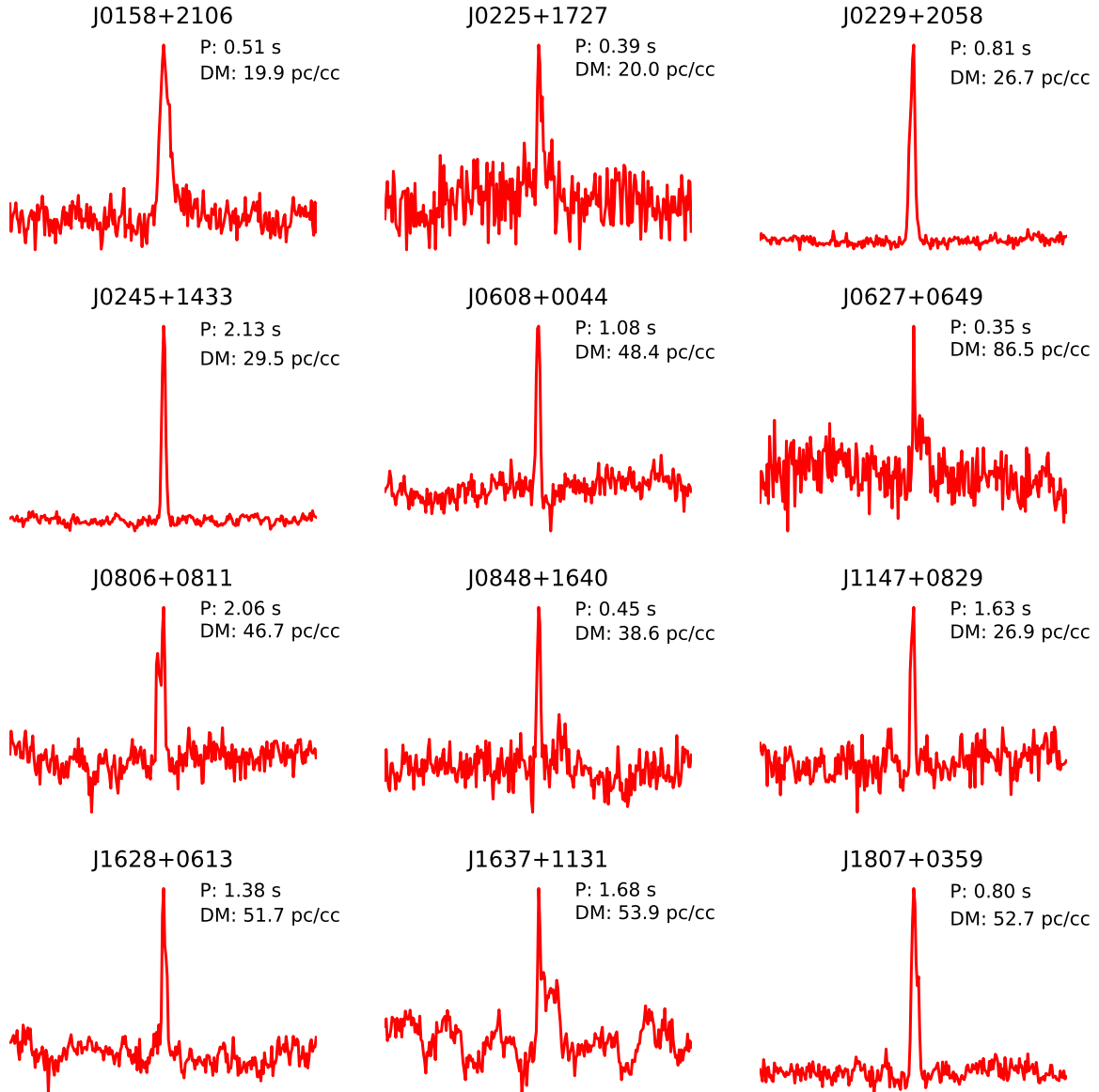


Figure 11. Epoch-averaged intensity profiles at 1380 MHz. We plot intensity on the y-axis and rotational phase on the x-axis. One full rotation is shown. Each profile has a resolution of 256 phase bins. We label each profile with the pulsar's period and DM.

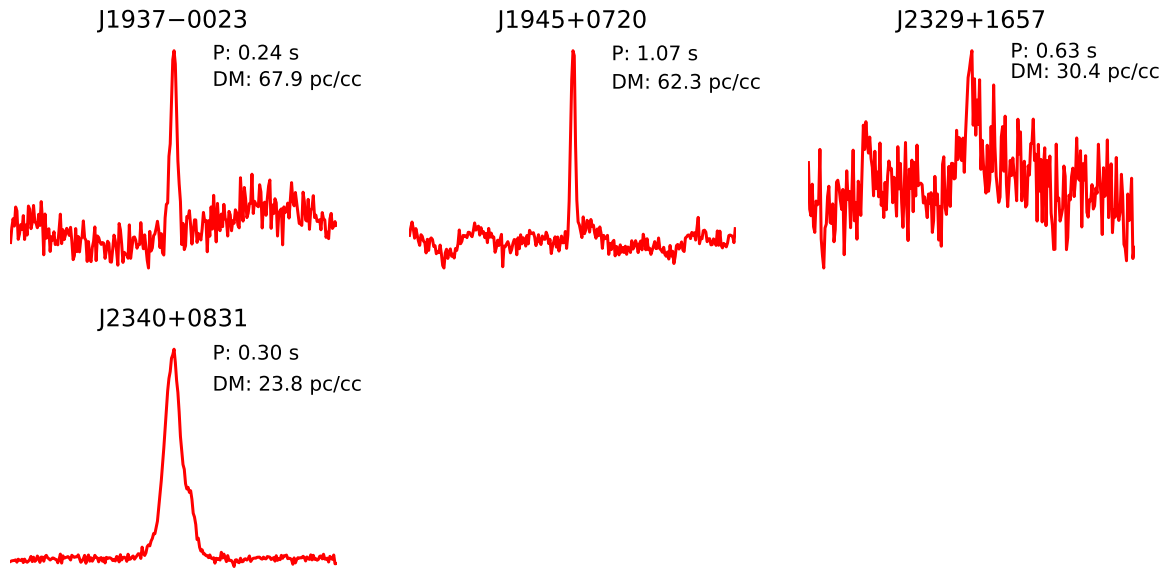


Figure 12. Epoch-averaged intensity profiles at 1380 MHz. We plot intensity on the y-axis and rotational phase on the x-axis. One full rotation is shown. Each profile has a resolution of 256 phase bins. We label each profile with the pulsar's period and DM.

REFERENCES

- Agazie, G., Anumarlapudi, A., Archibald, A. M., et al. 2023, *The Astrophysical Journal Letters*, 951, L8, doi: [10.3847/2041-8213/acdac6](https://doi.org/10.3847/2041-8213/acdac6)
- Agazie, G., Anumarlapudi, A., Archibald, A. M., et al. 2023, *ApJL*, 951, L8, doi: [10.3847/2041-8213/acdac6](https://doi.org/10.3847/2041-8213/acdac6)
- Agazie, G., Antoniadis, J., Anumarlapudi, A., et al. 2024, *The Astrophysical Journal*, 966, 105, doi: [10.3847/1538-4357/ad36be](https://doi.org/10.3847/1538-4357/ad36be)
- Alam, M. F., Arzoumanian, Z., Baker, P. T., et al. 2020, *The Astrophysical Journal Supplement Series*, 252, 4, doi: [10.3847/1538-4365/abc6a0](https://doi.org/10.3847/1538-4365/abc6a0)
- Andersen, B. C., & Ransom, S. M. 2018, *ApJL*, 863, L13, doi: [10.3847/2041-8213/aad59f](https://doi.org/10.3847/2041-8213/aad59f)
- Antoniadis, J., Kaplan, D. L., Stovall, K., et al. 2016, *ApJ*, 830, 36, doi: [10.3847/0004-637X/830/1/36](https://doi.org/10.3847/0004-637X/830/1/36)
- Arzamasskiy, L. I., Beskin, V. S., & Pirov, K. K. 2017, *Monthly Notices of the Royal Astronomical Society*, 466, 2325, doi: [10.1093/mnras/stw3139](https://doi.org/10.1093/mnras/stw3139)
- Barr, E. D., Dutta, A., Freire, P. C. C., et al. 2024, *Science*, 383, 275, doi: [10.1126/science.adg3005](https://doi.org/10.1126/science.adg3005)
- Basu, R., Mitra, D., & Melikidze, G. I. 2020, *The Astrophysical Journal*, 889, 133, doi: [10.3847/1538-4357/ab63c9](https://doi.org/10.3847/1538-4357/ab63c9)
- Basu, R., Mitra, D., Melikidze, G. I., & Skrzypczak, A. 2018, *Monthly Notices of the Royal Astronomical Society*, 482, 3757, doi: [10.1093/mnras/sty2846](https://doi.org/10.1093/mnras/sty2846)
- Belczynski, K., Lorimer, D. R., Ridley, J. P., & Curran, S. J. 2010, *Monthly Notices of the Royal Astronomical Society*, 407, 1245, doi: [10.1111/j.1365-2966.2010.16970.x](https://doi.org/10.1111/j.1365-2966.2010.16970.x)
- Burgay, M., Keith, M. J., Lorimer, D. R., et al. 2012, *Monthly Notices of the Royal Astronomical Society*, 429, 579, doi: [10.1093/mnras/sts359](https://doi.org/10.1093/mnras/sts359)
- Cady, E. B., & Ritchings, R. T. 1977, *Nature*, 269, 126, doi: [10.1038/269126a0](https://doi.org/10.1038/269126a0)
- Caleb, M., Heywood, I., Rajwade, K., et al. 2022, *Nature Astronomy*, 6, 828, doi: [10.1038/s41550-022-01688-x](https://doi.org/10.1038/s41550-022-01688-x)
- Caleb, M., Lenc, E., Kaplan, D. L., et al. 2024, *Nature Astronomy*, 8, 1159, doi: [10.1038/s41550-024-02277-w](https://doi.org/10.1038/s41550-024-02277-w)
- Chen, S., Caballero, R. N., Guo, Y. J., et al. 2021, *MNRAS*, 508, 4970, doi: [10.1093/mnras/stab2833](https://doi.org/10.1093/mnras/stab2833)
- Cordes, J. M., & Chatterjee, S. 2019, *Annual Review of Astronomy and Astrophysics*, 57, 417, doi: <https://doi.org/10.1146/annurev-astro-091918-104501>
- Cordes, J. M., & Lazio, T. J. W. 2002, *arXiv e-prints, astro*, doi: [10.48550/arXiv.astro-ph/0207156](https://doi.org/10.48550/arXiv.astro-ph/0207156)
- Cordes, J. M., & McLaughlin, M. A. 2003, *ApJ*, 596, 1142, doi: [10.1086/378231](https://doi.org/10.1086/378231)
- Cordes, J. M., Freire, P. C. C., Lorimer, D. R., et al. 2006, *ApJ*, 637, 446, doi: [10.1086/498335](https://doi.org/10.1086/498335)
- Cromartie, H. T., Fonseca, E., Ransom, S. M., et al. 2020, *Nature Astronomy*, 4, 72, doi: [10.1038/s41550-019-0880-2](https://doi.org/10.1038/s41550-019-0880-2)
- Dai, J.-P., Han, W., & Wang, N. 2024, *Research in Astronomy and Astrophysics*, 24, 085008, doi: [10.1088/1674-4527/ad484e](https://doi.org/10.1088/1674-4527/ad484e)
- Deneva, J. S., McLaughlin, M., Olszanski, T. E. E., et al. 2024, *The Astrophysical Journal Supplement Series*, 271, 23, doi: [10.3847/1538-4365/ad19da](https://doi.org/10.3847/1538-4365/ad19da)
- Deneva, J. S., Stovall, K., McLaughlin, M. A., et al. 2013, *The Astrophysical Journal*, 775, 51, doi: [10.1088/0004-637x/775/1/51](https://doi.org/10.1088/0004-637x/775/1/51)
- . 2016, *The Astrophysical Journal*, 821, 10, doi: [10.3847/0004-637x/821/1/10](https://doi.org/10.3847/0004-637x/821/1/10)
- Edwards, R. T., Hobbs, G. B., & Manchester, R. N. 2006, *Monthly Notices of the Royal Astronomical Society*, 372, 1549, doi: [10.1111/j.1365-2966.2006.10870.x](https://doi.org/10.1111/j.1365-2966.2006.10870.x)
- EPTA Collaboration and InPTA Collaboration, Antoniadis, J., Arumugam, P., et al. 2023, *A&A*, 678, A50, doi: [10.1051/0004-6361/202346844](https://doi.org/10.1051/0004-6361/202346844)
- Everett, J. E., & Weisberg, J. M. 2001, *ApJ*, 553, 341, doi: [10.1086/320652](https://doi.org/10.1086/320652)
- Fiore, W., Levin, L., McLaughlin, M. A., et al. 2023, *The Green Bank North Celestial Cap Survey. VIII. 21 New Pulsar Timing Solutions.* <https://arxiv.org/abs/2305.13624>
- Folkner, W. M., Williams, J. G., Boggs, D. H., Park, R. S., & Kuchynka, P. 2014, *Interplanetary Network Progress Report*, 42-196, 1
- Fonseca, E., Cromartie, H. T., Pennucci, T. T., et al. 2021, *ApJL*, 915, L12, doi: [10.3847/2041-8213/ac03b8](https://doi.org/10.3847/2041-8213/ac03b8)
- Freire, P. C. C., & Wex, N. 2024, *Living Reviews in Relativity*, 27, 5, doi: [10.1007/s41114-024-00051-y](https://doi.org/10.1007/s41114-024-00051-y)
- Górski, K. M., Hivon, E., Banday, A. J., et al. 2005, *ApJ*, 622, 759, doi: [10.1086/427976](https://doi.org/10.1086/427976)
- Han, J. L., Wang, C., Wang, P. F., et al. 2021, *Research in Astronomy and Astrophysics*, 21, 107, doi: [10.1088/1674-4527/21/5/107](https://doi.org/10.1088/1674-4527/21/5/107)
- Hankins, T. H. 2018, in *IAU Symposium, Vol. 337, Pulsar Astrophysics the Next Fifty Years*, ed. P. Weltevrede, B. B. P. Perera, L. L. Preston, & S. Sanidas, 29–32, doi: [10.1017/S1743921317007335](https://doi.org/10.1017/S1743921317007335)
- Harding, A. K. 2017, *Proceedings of the International Astronomical Union*, 13, 52, doi: [10.1017/s1743921318000509](https://doi.org/10.1017/s1743921318000509)
- Hewish, A., Bell, S. J., Pilkington, J. D. H., Scott, P. F., & Collins, R. A. 1968, *Nature*, 217, 709, doi: [10.1038/217709a0](https://doi.org/10.1038/217709a0)

- Johnston, S., & Romani, R. W. 2004, in IAU Symposium, Vol. 218, Young Neutron Stars and Their Environments, ed. F. Camilo & B. M. Gaensler, 315
- Kalberla, P. M. W., Burton, W. B., Hartmann, D., et al. 2005, *A&A*, 440, 775, doi: [10.1051/0004-6361:20041864](https://doi.org/10.1051/0004-6361:20041864)
- Keane, E. F., Kramer, M., Lyne, A. G., Stappers, B. W., & McLaughlin, M. A. 2011, *Monthly Notices of the Royal Astronomical Society*, 415, 3065, doi: [10.1111/j.1365-2966.2011.18917.x](https://doi.org/10.1111/j.1365-2966.2011.18917.x)
- Keith, M. J., Johnston, S., Weltevrede, P., & Kramer, M. 2010, *Monthly Notices of the Royal Astronomical Society*, 402, 745, doi: [10.1111/j.1365-2966.2009.15926.x](https://doi.org/10.1111/j.1365-2966.2009.15926.x)
- Keith, M. J., Jameson, A., van Straten, W., et al. 2010, *MNRAS*, 409, 619, doi: [10.1111/j.1365-2966.2010.17325.x](https://doi.org/10.1111/j.1365-2966.2010.17325.x)
- Kerr, M., Reardon, D. J., Hobbs, G., et al. 2020, *PASA*, 37, e020, doi: [10.1017/pasa.2020.11](https://doi.org/10.1017/pasa.2020.11)
- Kramer, M., Stairs, I. H., Manchester, R. N., et al. 2021, *Physical Review X*, 11, 041050, doi: [10.1103/PhysRevX.11.041050](https://doi.org/10.1103/PhysRevX.11.041050)
- Land, K., & Slosar, A. 2007, *PhRvD*, 76, 087301, doi: [10.1103/PhysRevD.76.087301](https://doi.org/10.1103/PhysRevD.76.087301)
- Lattimer, J. M. 2021, *Annual Review of Nuclear and Particle Science*, 71, 433, doi: [10.1146/annurev-nucl-102419-124827](https://doi.org/10.1146/annurev-nucl-102419-124827)
- Lazarus, P., Brazier, A., Hessels, J. W. T., et al. 2015, *The Astrophysical Journal*, 812, 81, doi: [10.1088/0004-637x/812/1/81](https://doi.org/10.1088/0004-637x/812/1/81)
- Lewis, E. F., Olszanski, T. E. E., Deneva, J. S., et al. 2023, *ApJ*, 956, 132, doi: [10.3847/1538-4357/acf99d](https://doi.org/10.3847/1538-4357/acf99d)
- Lorimer, D. R., & Kramer, M. 2004, *Handbook of Pulsar Astronomy*, Vol. 4
- Lorimer, D. R., Pol, N., Rajwade, K., et al. 2019, *Radio Pulsar Populations*, arXiv, doi: [10.48550/ARXIV.1903.06526](https://doi.org/10.48550/ARXIV.1903.06526)
- Maciesiak, K., Gil, J., & Ribeiro, V. A. R. M. 2011, *Monthly Notices of the Royal Astronomical Society*, 414, 1314, doi: [10.1111/j.1365-2966.2011.18471.x](https://doi.org/10.1111/j.1365-2966.2011.18471.x)
- Mahajan, N., van Kerkwijk, M. H., Main, R., & Pen, U.-L. 2018, *The Astrophysical Journal Letters*, 867, L2, doi: [10.3847/2041-8213/aae713](https://doi.org/10.3847/2041-8213/aae713)
- Manchester, R. N., Hobbs, G. B., Teoh, A., & Hobbs, M. 2005, *AJ*, 129, 1993, doi: [10.1086/428488](https://doi.org/10.1086/428488)
- Manchester, R. N., & Lyne, A. G. 1977, *MNRAS*, 181, 761, doi: [10.1093/mnras/181.4.761](https://doi.org/10.1093/mnras/181.4.761)
- Manchester, R. N., Lyne, A. G., Camilo, F., et al. 2001, *MNRAS*, 328, 17, doi: [10.1046/j.1365-8711.2001.04751.x](https://doi.org/10.1046/j.1365-8711.2001.04751.x)
- Martinez, J. G., Stovall, K., Freire, P. C. C., et al. 2015, *ApJ*, 812, 143, doi: [10.1088/0004-637X/812/2/143](https://doi.org/10.1088/0004-637X/812/2/143)
- Martinez, J. G., Stovall, K., Freire, P. C. C., et al. 2017, *The Astrophysical Journal*, 851, L29, doi: [10.3847/2041-8213/aa9d87](https://doi.org/10.3847/2041-8213/aa9d87)
- Martinez, J. G., Gentile, P., Freire, P. C. C., et al. 2019, *The Astrophysical Journal*, 881, 166, doi: [10.3847/1538-4357/ab2877](https://doi.org/10.3847/1538-4357/ab2877)
- McLaughlin, M., Kisseberth, N., Heatherly, S. A., et al. 2023, *Computing in Science & Engineering*, 25, 17, doi: [10.1109/MCSE.2023.3276811](https://doi.org/10.1109/MCSE.2023.3276811)
- McLaughlin, M., Kisseberth, N., Heatherly, S. A., et al. 2023, *Computing in Science and Engineering*, 25, 17, doi: [10.1109/MCSE.2023.3276811](https://doi.org/10.1109/MCSE.2023.3276811)
- McLaughlin, M. A., Lorimer, D. R., Champion, D. J., et al. 2004, in IAU Symposium, Vol. 218, Young Neutron Stars and Their Environments, ed. F. Camilo & B. M. Gaensler, 127, doi: [10.48550/arXiv.astro-ph/0310454](https://doi.org/10.48550/arXiv.astro-ph/0310454)
- McLaughlin, M. A., Lyne, A. G., Lorimer, D. R., et al. 2006, *Nature*, 439, 817, doi: [10.1038/nature04440](https://doi.org/10.1038/nature04440)
- Michilli, D., Bassa, C., Cooper, S., et al. 2019, *Monthly Notices of the Royal Astronomical Society*, 491, 725, doi: [10.1093/mnras/stz2997](https://doi.org/10.1093/mnras/stz2997)
- Ng, C., Wu, B., Ma, M., et al. 2020, *The Astrophysical Journal*, 903, 81, doi: [10.3847/1538-4357/abb94f](https://doi.org/10.3847/1538-4357/abb94f)
- Özel, F., & Freire, P. 2016, *ARA&A*, 54, 401, doi: [10.1146/annurev-astro-081915-023322](https://doi.org/10.1146/annurev-astro-081915-023322)
- Palliyaguru, N. T., Perera, B. B. P., McLaughlin, M. A., Osłowski, S., & Siebert, G. L. 2023, *Monthly Notices of the Royal Astronomical Society*, 520, 2747, doi: [10.1093/mnras/stad194](https://doi.org/10.1093/mnras/stad194)
- Pan, Z., Lu, J. G., Jiang, P., et al. 2023, *Nature*, 620, 961, doi: [10.1038/s41586-023-06308-w](https://doi.org/10.1038/s41586-023-06308-w)
- Pang, D., Goseva-Popstojanova, K., Devine, T., & McLaughlin, M. 2018, *Monthly Notices of the Royal Astronomical Society*, 480, 3302, doi: [10.1093/mnras/sty1992](https://doi.org/10.1093/mnras/sty1992)
- Parent, E., Sewalls, H., Freire, P. C. C., et al. 2022, *The Astrophysical Journal*, 924, 135, doi: [10.3847/1538-4357/ac375d](https://doi.org/10.3847/1538-4357/ac375d)
- Perera, B. B. P., DeCesar, M. E., Demorest, P. B., et al. 2019, *MNRAS*, 490, 4666, doi: [10.1093/mnras/stz2857](https://doi.org/10.1093/mnras/stz2857)
- Price, D. C., Flynn, C., & Deller, A. 2021, *PASA*, 38, e038, doi: [10.1017/pasa.2021.33](https://doi.org/10.1017/pasa.2021.33)
- Rankin, J. M. 1993, *ApJ*, 405, 285, doi: [10.1086/172361](https://doi.org/10.1086/172361)
- Ransom, S. 2011, *PRESTO: Pulsar Exploration and Search Toolkit*, Astrophysics Source Code Library, record ascl:1107.017. <http://ascl.net/1107.017>
- Ransom, S. M. 2001, PhD thesis, Harvard University, Massachusetts
- Ransom, S. M., Eikenberry, S. S., & Middleditch, J. 2002, *AJ*, 124, 1788, doi: [10.1086/342285](https://doi.org/10.1086/342285)

- Reardon, D. J., Zic, A., Shannon, R. M., et al. 2023, *The Astrophysical Journal Letters*, 951, L6, doi: [10.3847/2041-8213/acdd02](https://doi.org/10.3847/2041-8213/acdd02)
- Ridolfi, A., Gautam, T., Freire, P. C. C., et al. 2021, *MNRAS*, 504, 1407, doi: [10.1093/mnras/stab790](https://doi.org/10.1093/mnras/stab790)
- Rosen, R., Swiggum, J., McLaughlin, M. A., et al. 2013, *ApJ*, 768, 85, doi: [10.1088/0004-637X/768/1/85](https://doi.org/10.1088/0004-637X/768/1/85)
- Sanidas, S., Cooper, S., Bassa, C. G., et al. 2019, *A&A*, 626, A104, doi: [10.1051/0004-6361/201935609](https://doi.org/10.1051/0004-6361/201935609)
- Sob'yanin, D. N. 2023, *Phys. Rev. D*, 107, L081301, doi: [10.1103/PhysRevD.107.L081301](https://doi.org/10.1103/PhysRevD.107.L081301)
- Stovall, K., Lynch, R. S., Ransom, S. M., et al. 2014, *ApJ*, 791, 67, doi: [10.1088/0004-637X/791/1/67](https://doi.org/10.1088/0004-637X/791/1/67)
- Stovall, K., Freire, P. C. C., Antoniadis, J., et al. 2019, *ApJ*, 870, 74, doi: [10.3847/1538-4357/aaf37d](https://doi.org/10.3847/1538-4357/aaf37d)
- Swiggum, J. K., Pleunis, Z., Parent, E., et al. 2023, *The Astrophysical Journal*, 944, 154, doi: [10.3847/1538-4357/acb43f](https://doi.org/10.3847/1538-4357/acb43f)
- Szary, A., & van Leeuwen, J. 2017, *The Astrophysical Journal*, 845, 95, doi: [10.3847/1538-4357/aa803a](https://doi.org/10.3847/1538-4357/aa803a)
- Szary, A., van Leeuwen, J., Weltevrede, P., & Maan, Y. 2020, *The Astrophysical Journal*, 896, 168, doi: [10.3847/1538-4357/ab9226](https://doi.org/10.3847/1538-4357/ab9226)
- Tauris, T. M., & van den Heuvel, E. P. J. 2023, *Physics of Binary Star Evolution. From Stars to X-ray Binaries and Gravitational Wave Sources*
- Tauris, T. M., Kramer, M., Freire, P. C. C., et al. 2017, *ApJ*, 846, 170, doi: [10.3847/1538-4357/aa7e89](https://doi.org/10.3847/1538-4357/aa7e89)
- Taylor, J. H. 1992, *Philosophical Transactions of the Royal Society of London Series A*, 341, 117, doi: [10.1098/rsta.1992.0088](https://doi.org/10.1098/rsta.1992.0088)
- Teixeira, M. M., Rankin, J. M., Wright, G. A. E., & Dyks, J. 2015, *Monthly Notices of the Royal Astronomical Society*, 455, 3201, doi: [10.1093/mnras/stv2520](https://doi.org/10.1093/mnras/stv2520)
- Thornton, D., Stappers, B., Bailes, M., et al. 2013, *Science*, 341, 53, doi: [10.1126/science.1236789](https://doi.org/10.1126/science.1236789)
- Turner, J. E., McLaughlin, M. A., Cordes, J. M., et al. 2021, *The Astrophysical Journal*, 917, 10, doi: [10.3847/1538-4357/abfafa](https://doi.org/10.3847/1538-4357/abfafa)
- Tyulbashev, V. S., & Malofeev, V. M. 2018, *A&A*, 618, A70, doi: [10.1051/0004-6361/201833102](https://doi.org/10.1051/0004-6361/201833102)
- van Leeuwen, J., & Timokhin, A. N. 2012, 752, 155, doi: [10.1088/0004-637X/752/2/155](https://doi.org/10.1088/0004-637X/752/2/155)
- Verbiest, J. P. W., Lentati, L., Hobbs, G., et al. 2016, *Monthly Notices of the Royal Astronomical Society*, 458, 1267, doi: [10.1093/mnras/stw347](https://doi.org/10.1093/mnras/stw347)
- Wang, N., Manchester, R. N., & Johnston, S. 2007, *Monthly Notices of the Royal Astronomical Society*, 377, 1383, doi: [10.1111/j.1365-2966.2007.11703.x](https://doi.org/10.1111/j.1365-2966.2007.11703.x)
- Wang, P. F., Han, J. L., Xu, J., et al. 2023, *FAST pulsar database: I. Polarization profiles of 682 pulsars*. <https://arxiv.org/abs/2307.10340>
- Weltevrede, P., & Johnston, S. 2008, *Monthly Notices of the Royal Astronomical Society*, 387, 1755, doi: [10.1111/j.1365-2966.2008.13382.x](https://doi.org/10.1111/j.1365-2966.2008.13382.x)
- Wright, G., & Weltevrede, P. 2016, *Monthly Notices of the Royal Astronomical Society*, 464, 2597, doi: [10.1093/mnras/stw2498](https://doi.org/10.1093/mnras/stw2498)
- Yao, J. M., Manchester, R. N., & Wang, N. 2017, *ApJ*, 835, 29, doi: [10.3847/1538-4357/835/1/29](https://doi.org/10.3847/1538-4357/835/1/29)
- Zonca, A., Singer, L., Lenz, D., et al. 2019, *Journal of Open Source Software*, 4, 1298, doi: [10.21105/joss.01298](https://doi.org/10.21105/joss.01298)

APPENDIX

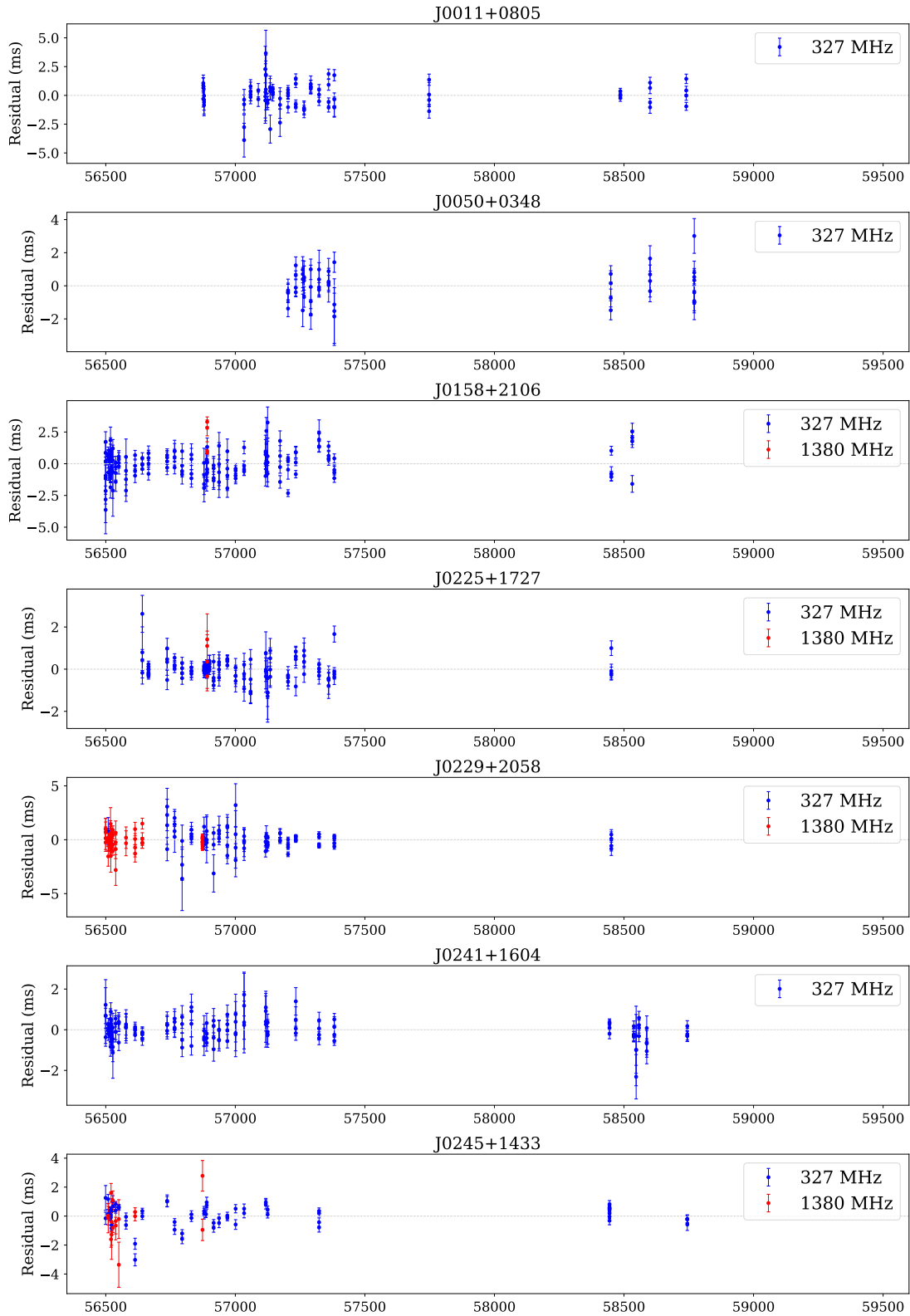


Figure 13. Residuals for individual timing solutions. We plot the postfit residual on the y-axis and the MJD on the x-axis. Blue coloring corresponds to data taken at 327 MHz while red coloring is used for 1380 MHz observations.

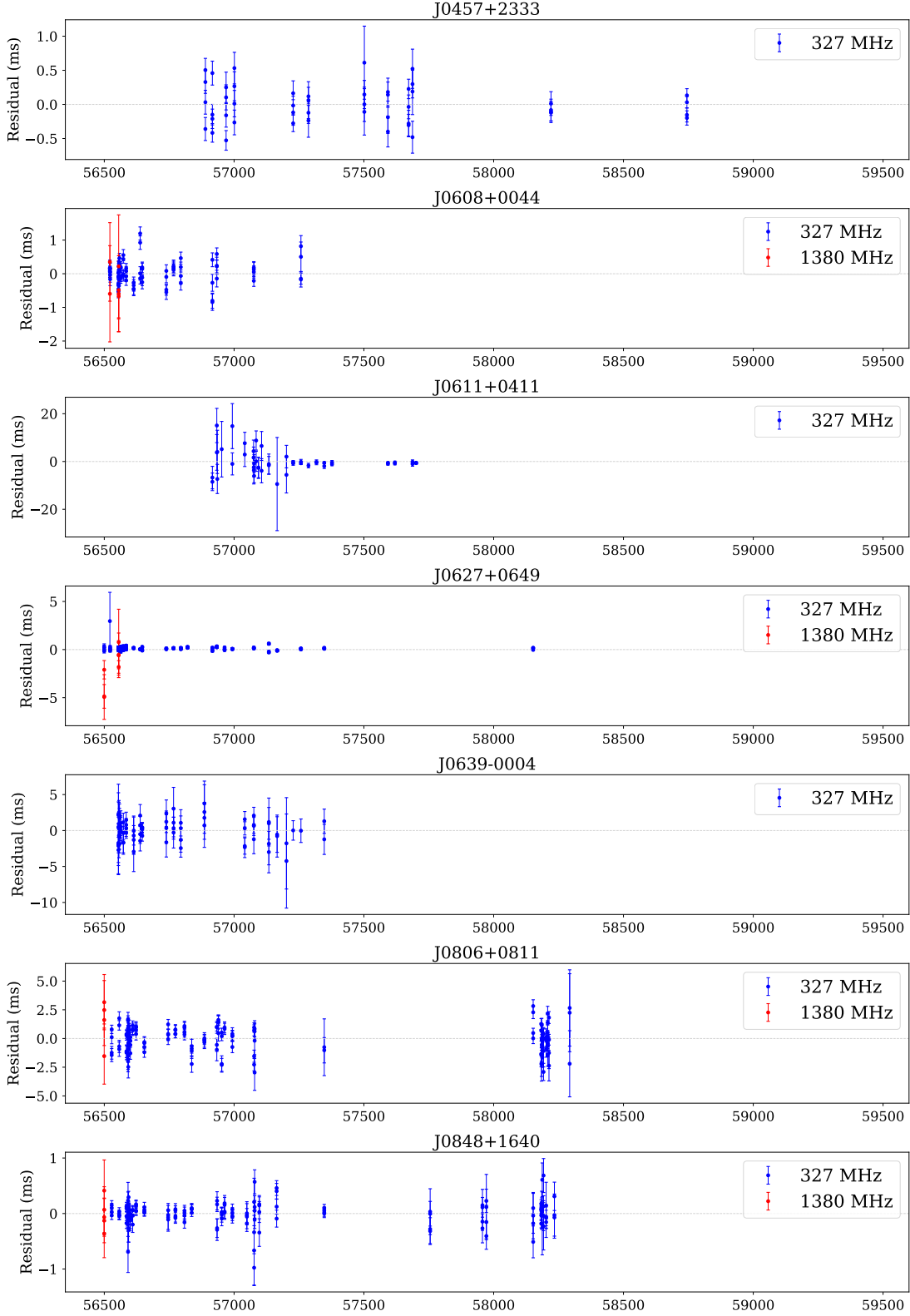


Figure 14. Residuals for individual timing solutions. We plot the postfit residual on the y-axis and the MJD on the x-axis. Blue coloring corresponds to data taken at 327 MHz while red coloring is used for 1380 MHz observations.

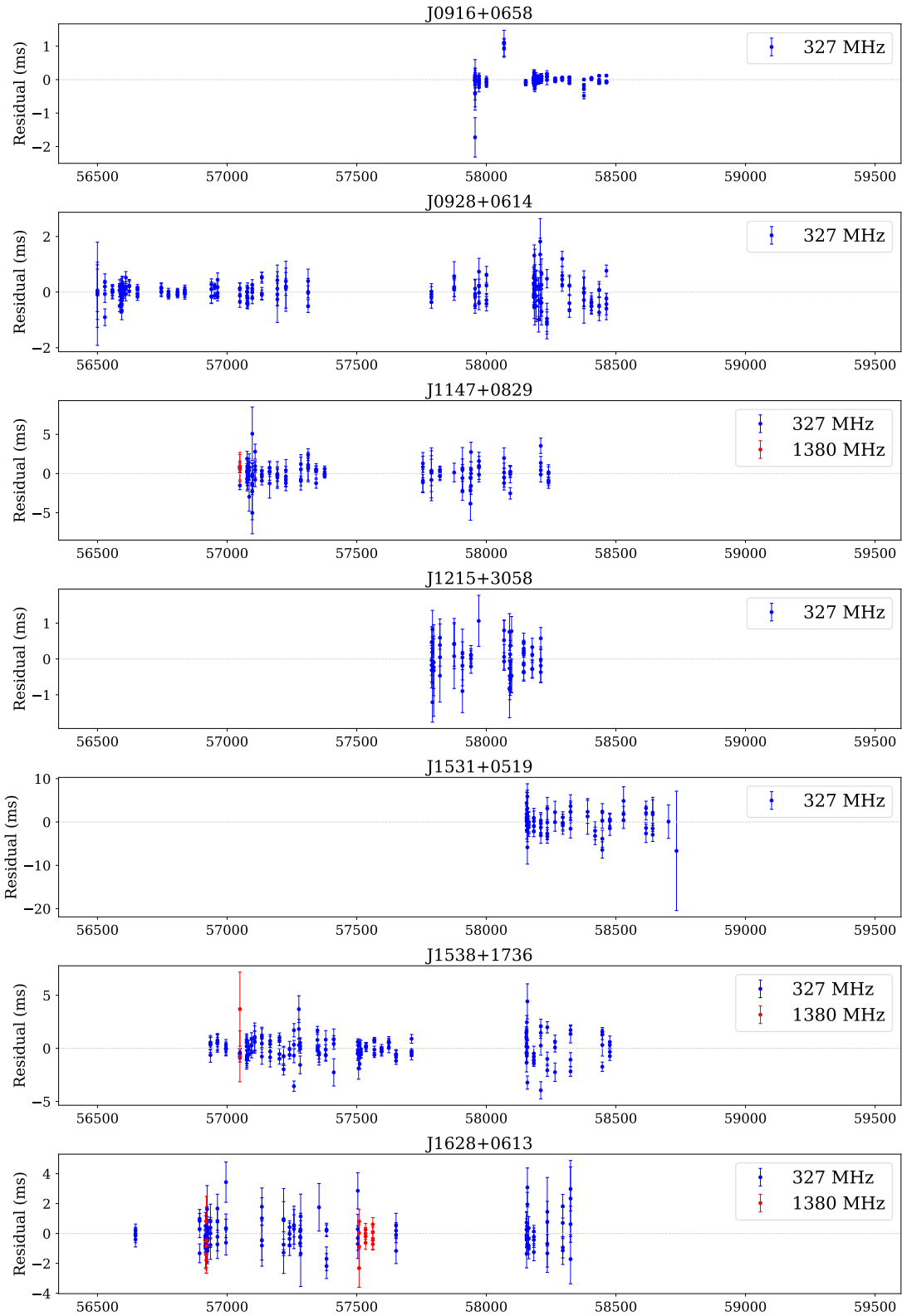


Figure 15. Residuals for individual timing solutions. We plot the postfit residual on the y-axis and the MJD on the x-axis. Blue coloring corresponds to data taken at 327 MHz while red coloring is used for 1380 MHz observations.

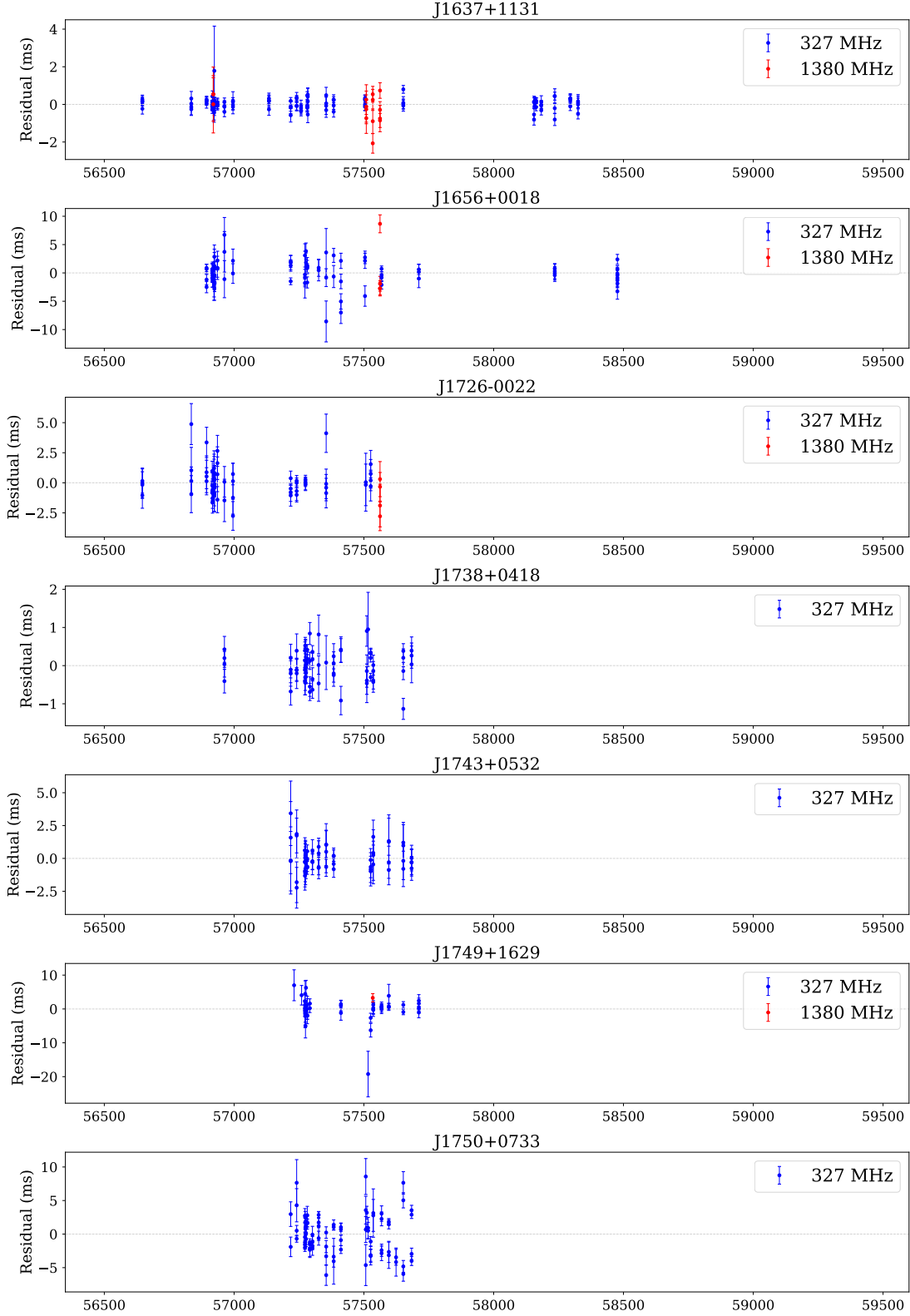


Figure 16. Residuals for individual timing solutions. We plot the postfit residual on the y-axis and the MJD on the x-axis. Blue coloring corresponds to data taken at 327 MHz while red coloring is used for 1380 MHz observations.

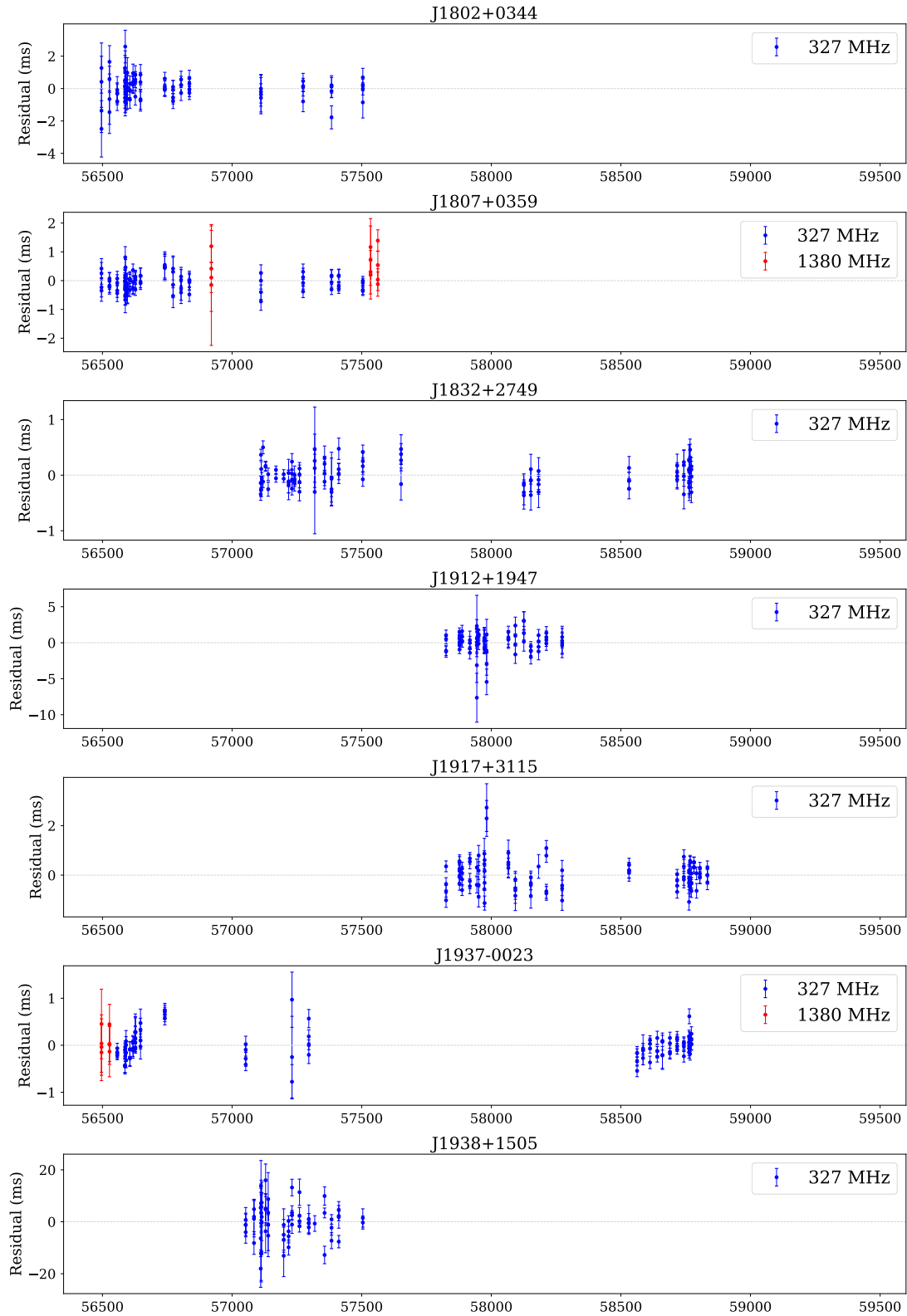


Figure 17. Residuals for individual timing solutions. We plot the postfit residual on the y-axis and the MJD on the x-axis. Blue coloring corresponds to data taken at 327 MHz while red coloring is used for 1380 MHz observations.

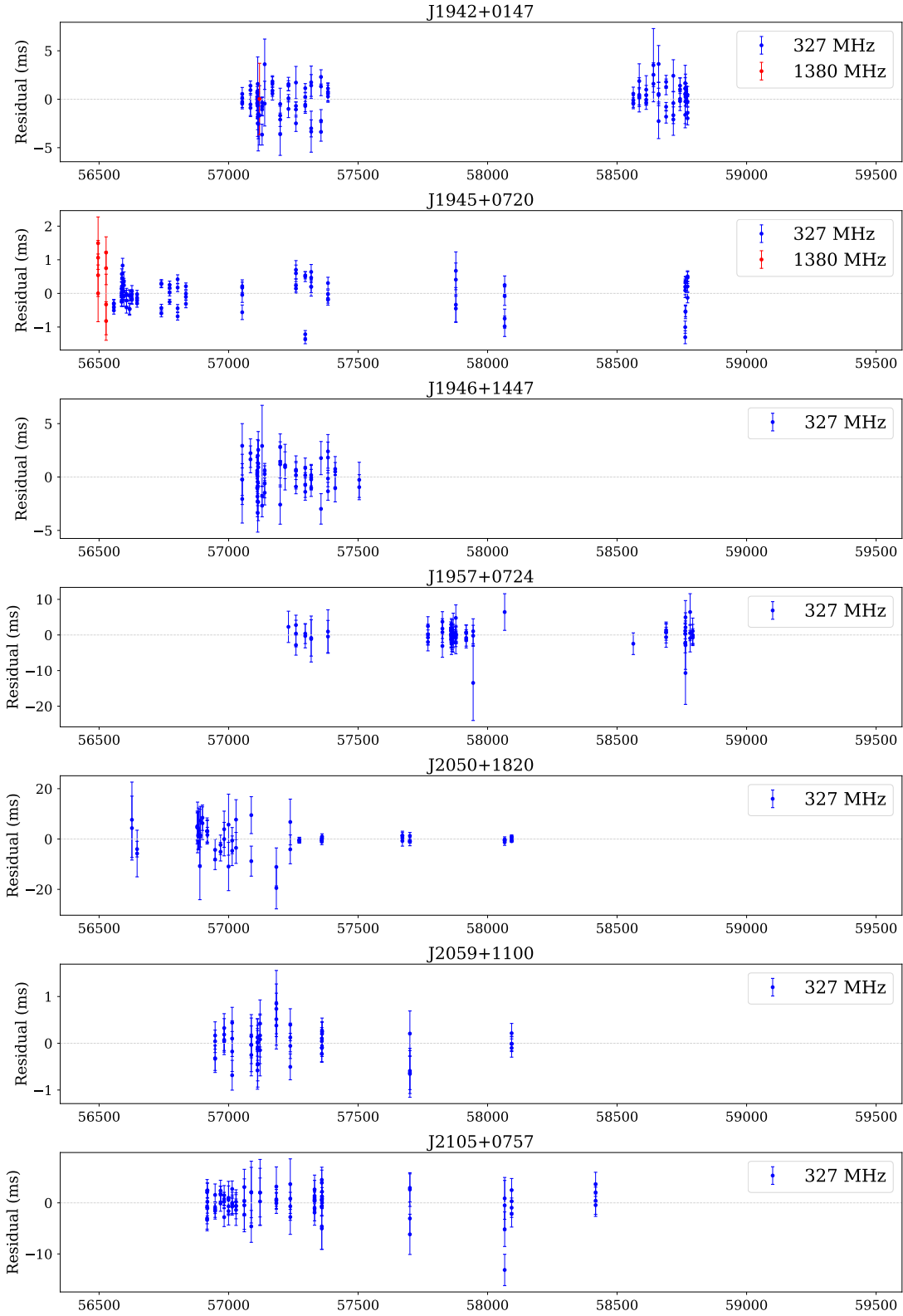


Figure 18. Residuals for individual timing solutions. We plot the postfit residual on the y-axis and the MJD on the x-axis. Blue coloring corresponds to data taken at 327 MHz while red coloring is used for 1380 MHz observations.

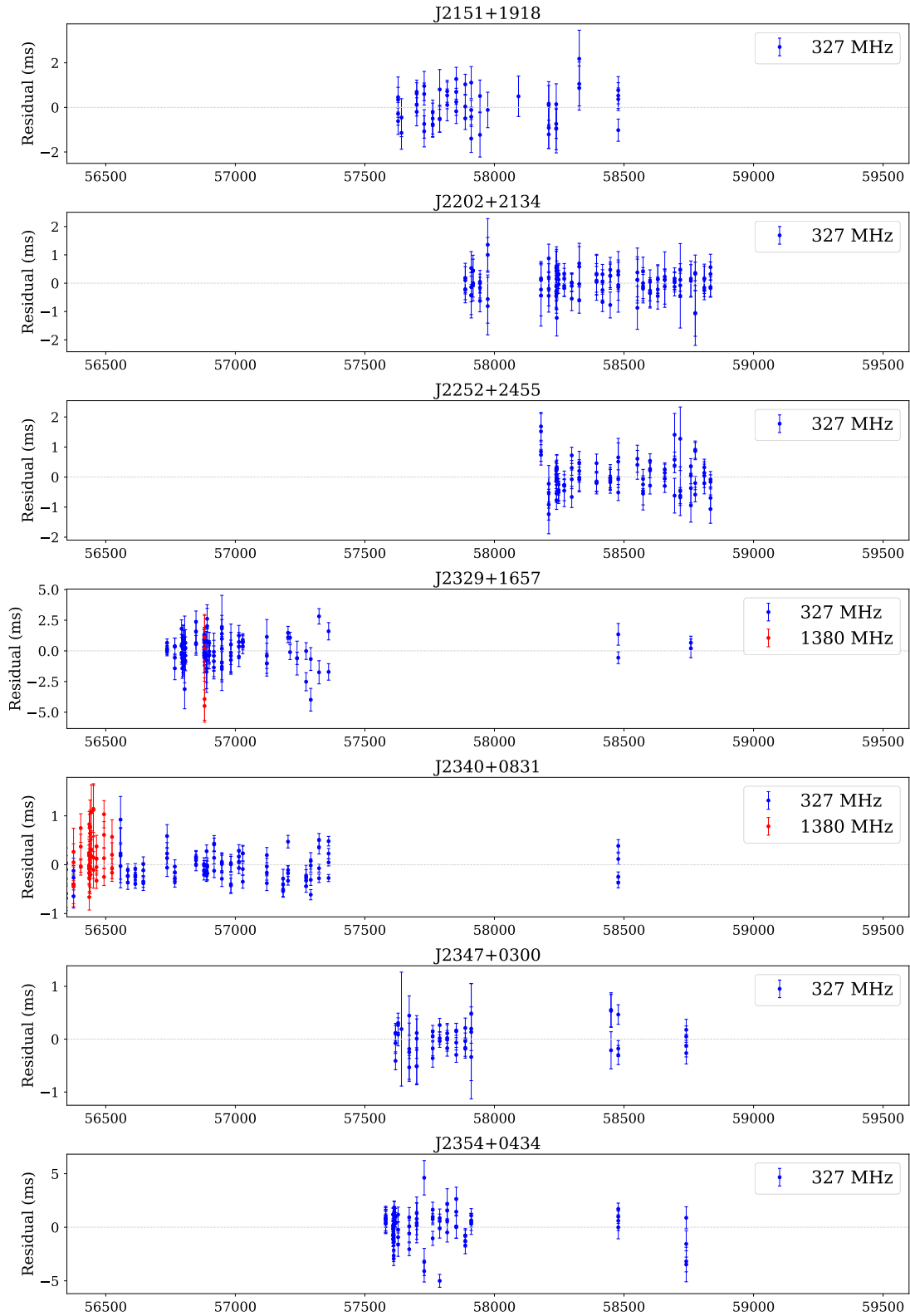


Figure 19. Residuals for individual timing solutions. We plot the postfit residual on the y-axis and the MJD on the x-axis. Blue coloring corresponds to data taken at 327 MHz while red coloring is used for 1380 MHz observations.